Charge transfer transitions in multiferroic $BiFeO_3$ and related ferrite insulators

R. V. Pisarev,[1] A. S. Moskvin,[2] A. M. Kalashnikova,[1,3] and Th. Rasing[3]
[1]*Ioffe Physical-Technical Institute, Russian Academy of Sciences, 194021 St. Petersburg, Russia*
[2]*Ural State University, 620083 Ekaterinburg, Russia*
[3]*Institute for Molecules and Materials, Radboud University Nijmegen, Heyendaalseweg 135, 6525 AJ Nijmegen, The Netherlands*
(Received 20 February 2009; revised manuscript received 4 May 2009; published 23 June 2009)

The optical response of the technologically interesting multiferroic $BiFeO_3$ and related complex iron oxides, having high Néel or Curie temperature, is studied in the wide spectral range from 0.6 up to 5.8 eV by means of spectroscopic ellipsometry. The investigated iron oxides have different crystal symmetry with FeO_6 octahedral and FeO_4 tetrahedral centers distorted to a certain degree. One of the two groups of materials includes $BiFeO_3$, $ErFeO_3$, $Y_{.95}Bi_{.05}FeO_3$, α-Fe_2O_3, $Fe_{2-x}Ga_xO_3$, and Fe_3BO_6 in which iron Fe^{3+} ions occupy only octahedral centrosymmetric or noncentrosymmetric positions and distortions range of 1–20 %. The second group includes $LiFe_5O_8$, $BaFe_{12}O_{19}$, $Sm_3Fe_5O_{12}$, and $Ca_2Fe_2O_5$ in which Fe^{3+} ions occupy both octahedral and tetrahedral positions with a rising tetra/ortho ratio. We show that in the spectral range up to ~3.7 eV, the optical response is dominated by *p-d* charge transfer (CT) transitions, while at $E>3.7$ eV both *p-d* and *d-d* CT transitions are revealed. At variance with several previous investigations, we present a correct and unified assignment of different dipole-allowed and dipole-forbidden CT transitions. All the ferrites investigated are CT insulators with the band gap determined by a dipole-forbidden *p-d* CT transition $t_{1g}\rightarrow t_{2g}$, forming a ~2.5 eV band on the tail of a strong 3.0 eV band assigned to dipole-allowed *p-d* CT transitions $t_{2u}(\pi)\rightarrow t_{2g}$ in octahedral FeO_6 centers. A noticeable enhancement of the optical response in $BiFeO_3$ at ~4 eV as compared with other related iron oxides is attributed to CT transitions within the Bi-O bonds. We report an observation of unexpected midinfrared CT bands in calcium ferrite $Ca_2Fe_2O_5$ and an enhanced structureless spectral weight in a wide range below the main CT bands in $BiFeO_3$ with a remarkable smearing of the fundamental absorption edge. All these anomalies are assigned to CT instabilities accompanied by a self-trapping of *p-d* CT excitons and nucleation of electron-hole droplets. The optical detection of this CT instability agrees with the observation of a metal-insulator transition in bismuth ferrite.

DOI: 10.1103/PhysRevB.79.235128 PACS number(s): 78.20.Bh, 78.20.Ci, 75.50.Ee, 77.80.−e

I. INTRODUCTION

Multiferroic materials with two or more coexisting order parameters are known since the 1960s (see review papers).[1–4] The possible interactions between different order parameters make these materials promising candidates for the development of new spintronics and optoelectronics devices. However, earlier attempts to develop devices based on the mutual control of the magnetic, electric, and deformation states appeared to be unsuccessful because of the small values of the cross coupling between the respective order parameters. Only recently, the discovery of new compounds and multiphase structures exhibiting large multiferroic interactions renewed interest in this group of materials. Good examples are the most actively studied rare-earth (R) hexagonal and perovskite manganites $R\mathrm{MnO_3}$ and orthorhombic manganites $R\mathrm{Mn_2O_5}$.[5–9] However, the majority of multiferroic materials extensively studied so far possesses magnetic transition temperatures far below room temperature. Though demonstrating interesting new physics, they most probably are of no interest for practical applications.

Among the materials exhibiting multiferroic properties above room temperature, the complex iron oxides based on octahedrally and/or tetrahedrally coordinated Fe^{3+} ion are of interest, as their electronic structure with half-filled t_{2g}^3 and e_g^2 orbitals favors strong exchange interaction and the highest magnetic transition temperatures in comparison to other 3*d* transition-metals oxides. Examples of such materials are lithium ferrite $LiFe_5O_8$ in which the magnetoelectric effect[10] and the optical magnetoelectric effect[11] were observed, thin films of bismuth-substituted iron garnets $R_{1-x}Bi_xFe_5O_{12}$ with giant optical magnetoelectric effects,[12] gallium ferrite $GaFeO_3$,[13–15] and the recently reported magnetoelectric hexaferrites $Ba_{0.5}Sr_{1.5}Zn_2Fe_{12}O_{22}$ (Ref. 16) and $Ba_2Mg_2Fe_{12}O_{22}$.[17]

However, the most prominent multiferroic among all known iron oxides is the bismuth ferrite $BiFeO_3$. A large amount of literature has been published in recent years concerning the physical properties of bulk crystals and thin films of $BiFeO_3$ (see, e.g., the most recent papers and references therein).[18,19] Alongside with the multiferroicity a metal-insulator transition under high pressure was reported.[18] On the other hand, such a transition was also reported under atmospheric pressure at high temperature,[19] which is quite unusual for the Fe^{3+} oxides. $BiFeO_3$ reveals unique multiferroic and optical properties that imply its potential as a photovoltaic material[20] and suggests it to be suitable for novel optoelectronic devices. These experimental observations along with recent theoretical predictions of important electronic contributions to the multiferroic properties are a strong motivation for more detailed studies of its electronic structure. There have been several measurements of the band gap of $BiFeO_3$ using UV-visible absorption spectroscopy and ellipsometry on polycrystalline $BiFeO_3$ films, epitaxial $BiFeO_3$ films grown by pulsed-laser deposition, nanowires, nanotubes, and bulk single crystals. Reported band-gap values vary from 2.5 up to 2.8 eV.[18–22]

All theoretical[23–26] and very recent experimental studies[20,27,28] of $BiFeO_3$ are focused on the characterization of the band-gap and near-band-gap states as well as the puzzling metal-insulator transition.[18,19] Recent transmittance,[20,21] absorption, and cathodoluminescence spectra[27] revealed a low-energy near-band-gap optical feature near 2.5 eV. This was attributed to defect states due to oxygen vacancies though Basu *et al.*[20] could not discern whether the feature was related to a low-lying electronic structure or whether it had an excitonic character. Theoretical understanding of the in-gap states is of primary importance for conductivity mechanisms and for mechanisms of intrinsic leakage currents in multiferroics. A better understanding of the mechanisms governing the optical response may enable researchers to engineer the band gap and conductivity to enhance the photoferroelectric properties.[20]

First-principles local spin-density approximation LSDA $+U$ calculations predict $BiFeO_3$ to be an indirect-band insulator with $E_g=2.0$ eV, this value being subject to the parameters chosen.[23,24] More recently, Clark and Robertson[26] employed the screened-exchange density-functional theory approximation to estimate the band gap of $BiFeO_3$. Their calculation yielded a band gap of approximately 2.8 eV. However, no comprehensive analysis of the spectral features and mechanisms governing the optical response of $BiFeO_3$ have been reported yet. At the same time this kind of information is of primary importance for the elucidation of the actual electronic states and a theoretical understanding of the mechanism(s) of the strong magnetoelectric coupling, in particular, the role of the electronic contribution to the multiferroic properties which may be quite important and in some cases comparable to the lattice contribution.[29,30] Indeed, the mechanisms of electric polarization, including its spin-dependent part, and the mechanisms specifying the optical response in $3d$ oxides have much in common.[30–32] Both are dominated by the p-d and d-d charge transfer (CT) transitions that makes its theoretical and experimental study a challenging task.

Thus, experimental and theoretical investigations of the electronic structure of $BiFeO_3$, especially the CT transitions, the band-gap and in-gap states are of particular importance for both a better scientific understanding as well as potential technological applications. In this paper, we report results of a theoretical analysis of the CT transitions and a comparative experimental spectroscopic study of the dielectric function of $BiFeO_3$ and several other related Fe^{3+} iron oxides with perovskite and more complicated crystal structures. We discuss the possible role of the CT states in the metal-insulator transition recently observed in $BiFeO_3$ at high temperature[19] and under high hydrostatic pressure.[18]

The paper is organized as follows. In Sec. II we present a theoretical analysis of the p-d and d-d charge transfer transitions in iron oxides. Experimental results of the spectroscopic study are presented in Sec. III following with a discussion in Sec. IV. In Sec. V we discuss the possible role of the CT states in the metal-insulator transition.

II. THEORETICAL CONSIDERATION OF CHARGE TRANSFER TRANSITIONS IN IRON OXIDES

Conventional classification of optically active transitions in solids implies both various intraband and interband transitions in the bandlike picture and various intra-atomic and interatomic transitions in the atomiclike picture. Intra-atomic transitions, in their turn, are classified according to the formally forbidden intraconfigurational ones, e.g., d-d, or crystal-field transitions, and to the interconfigurational transitions such as the strong allowed $3d$-$4p$ ones. All the interatomic transitions are driven by the charge transfer and may be termed as the CT ones. Below we focus on the p-d CT transitions in $3d$ oxides driven by the O $2p$-Me $3d$ electron transfer and the d-d CT transitions driven by the Me_1 $3d$-Me_2 $3d$ intersite electron transfer. Usually these ones are termed CT transitions and Mott-Hubbard transitions, respectively. It should be noted that when we proceed with the metal-oxygen centers CuO_4, MnO_6,… as building blocks of the crystal and electronic structure, the p-d and d-d CT transitions may be termed as one-center and two-center CT transitions, respectively. Note that for the metal-oxygen centers with well-developed covalent effects, all the one-center transitions are somehow associated with the interatomic p-d or p-p CT transitions.

A. One-center p-d charge transfer transitions

First we address the electronic structure and one-center p-d charge transfer transitions in octahedral $3d$-metal-oxygen $Fe^{3+}O_6$ centers in a perovskitelike surrounding. Five Fe $3d$ and 18 oxygen O $2p$ atomic orbitals in the octahedral FeO_6 complex with point symmetry group O_h form both hybrid Fe $3d$-O $2p$ bonding and antibonding e_g and t_{2g} molecular orbitals (MOs) and purely oxygen nonbonding $a_{1g}(\sigma)$, $t_{1g}(\pi)$, $t_{1u}(\sigma)$, $t_{1u}(\pi)$, and $t_{2u}(\pi)$ orbitals. Nonbonding $t_{1u}(\sigma)$ and $t_{1u}(\pi)$ orbitals with the same symmetry are hybridized due to the oxygen-oxygen O $2p\pi$-O $2p\pi$ transfer. The relative energy positions of different nonbonding oxygen orbitals are of primary importance for the spectroscopy of the oxygen-$3d$-metal charge transfer. This is first determined by the bare energy separation $\Delta\epsilon_{2p\pi\sigma}=\epsilon_{2p\pi}-\epsilon_{2p\sigma}$ between O $2p\pi$ and O $2p\sigma$ electrons. Since the O $2p\sigma$ orbital points toward the two neighboring positive $3d$ ions, an electron in this orbital has its energy lowered by the Madelung potential as compared with the O $2p\pi$ orbitals, which are perpendicular to the respective $3d$-O-$3d$ axes.

Thus, Coulomb interaction favors the positive sign of the $\pi-\sigma$ separation $\epsilon_{p\pi}-\epsilon_{p\sigma}$ which numerical value can be easily estimated within the frame of the well-known point-charge model. It appears to be on the order of 1.0 eV. In the first approximation, all the $\gamma(\pi)$ states $t_{1g}(\pi), t_{1u}(\pi), t_{2u}(\pi)$ have the same energy. However, the O $2p\pi$-O $2p\pi$ transfer yields an energy correction to the bare energies, with the largest value and positive sign for the $t_{1g}(\pi)$ state. The energy of the $t_{1u}(\pi)$ state drops due to hybridization with the cation $4pt_{1u}(\pi)$ state. In other words, the $t_{1g}(\pi)$ state is believed to be the highest nonbonding oxygen state, thus forming the first electron removal from the oxygen states.[33,34] For a semiquantitative analysis we use quantum-chemical calculations[34] for $[Fe^{3+}O_6]^{9-}$ centers in $LaFeO_3$, which leads to following energy separations: $\Delta[t_{1g}(\pi)-t_{2u}(\pi)]\approx 0.8$ eV; $\Delta[t_{1g}(\pi)-t_{1u}(\pi)]\approx 1.8$ eV; and $\Delta[t_{1g}(\pi)-t_{1u}(\sigma)]\approx 3.0$ eV. This is believed to be a rather reasonable choice of the en-

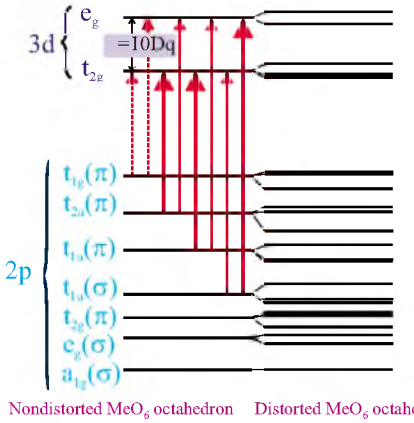

FIG. 1. (Color online) The diagram of Fe $3d$-O $2p$ molecular orbitals for the FeO_6 octahedral center. The O $2p$-Fe $3d$ charge transfer transitions are shown by arrows: strong dipole-allowed $\sigma-\sigma$ and $\pi-\pi$ by thick solid arrows; weak dipole-allowed $\pi-\sigma$ and $\sigma-\pi$ by thin solid arrows; and weak dipole-forbidden low-energy transitions by thin dashed arrows, respectively.

ergy parameters because the purely oxygen states mainly depend on the crystalline environment. For illustration, in Fig. 1 we show the energy spectrum of the $3d$-$2p$ manifold for the $[FeO_6]^{9-}$ octahedral complex, with the relative energy position of the levels according to the quantum-chemical calculations in a lattice environment typical for perovskitelike $LaFeO_3$.[34,35]

It should be emphasized once more that the top of the oxygen electron band is composed of the O $2p\pi$ nonbonding orbitals. This determines their role in several physical properties of the $3d$ perovskites.

The *conventional* ground-state electronic structure of octahedral $Fe^{3+}O_6$ complexes is associated with the configuration of the completely filled O $2p$ shells and half-filled Fe $3d$ shell. The typical high-spin (HS) ground-state configuration and crystalline term for Fe^{3+} in the octahedral crystal field or for the octahedral $[FeO_6]^{9-}$ center is $t_{2g}^3 e_g^2$ and ${}^6A_{1g}$, respectively.

The *unconventional* electronic configuration of the octahedral FeO_6 complexes is associated with a *charge transfer state* with one hole in the O $2p$ shells. The excited CT configuration $\underline{\gamma}_{2p}^1 3d^{n+1}$ arises from the transition of an electron from the predominantly anionic MO (the γ_{2p} hole in the core of the anionic MO being hereby produced) into an empty $3d$-type MO (t_{2g} or e_g). The transition between the ground configuration and the excited one can be presented as a $\gamma_{2p} \rightarrow 3d(t_{2g}, e_g)$ CT transition.

The CT configuration consists of two partially filled subshells, the ligand γ_{2p}, and the cation $3d(t_{2g}^{n_1} e_g^{n_2})$ shell, respectively. In the case of CT states in the $[FeO_6]^{9-}$ center, this configuration corresponds nominally to the Fe^{2+} ion. It should be emphasized that the oxygen hole, having occupied the *nonbonding* γ_{2p} orbital, interacts *ferromagnetically* with the $3d(t_{2g}^{n_1} e_g^{n_2})$ shell. This rather strong ferromagnetic coupling results in the Hund rule for the CT configurations and provides the high-spin ground states. The presence of the oxygen hole moving around the $3d$ ion in the CT state can provide a strong screening of both the $3d$ crystal-field and the intra-atomic electron-electron repulsion, with a renormalization of the appropriate correlation Racah parameters A, B, C and the crystal-field splitting parameter Dq.

The even-parity molecular orbital $\gamma_g \mu = N_{\gamma_g}(3d\gamma_g\mu + \lambda_{\gamma_g} 2p\gamma_g\mu)$ with the $3d$-$2p$ hybrid structure and the purely oxygen odd-parity molecular orbital $\gamma_u\mu \equiv 2p\gamma_u\mu$, both include the symmetry superposition of the on-site ligands O $2p$ orbitals. The electric dipole matrix element will therefore be a sum of *local* and *nonlocal* terms composed from one-site and two-site (d-p and p-p) integrals, respectively. In the framework of a simple "local" approximation[35] that implies the full neglect of all the many-center integrals, we obtain

$$\langle t_{2u}(\pi)\|\hat{d}\|e_g\rangle = 0; \quad \langle t_{2u}(\pi)\|\hat{d}\|t_{2g}\rangle = -i\sqrt{\frac{3}{2}}\lambda_\pi d,$$

$$\langle t_{1u}(\sigma)\|\hat{d}\|t_{2g}\rangle = 0; \quad \langle t_{1u}(\sigma)\|\hat{d}\|e_g\rangle = -\frac{2}{\sqrt{3}}\lambda_\sigma d,$$

$$\langle t_{1u}(\pi)\|\hat{d}\|e_g\rangle = 0; \quad \langle t_{1u}(\pi)\|\hat{d}\|t_{2g}\rangle = \sqrt{\frac{3}{2}}\lambda_\pi d. \qquad (1)$$

Here, $\lambda_\sigma \sim t_{pd\sigma}/\Delta_{pd}$, $\lambda_\pi \sim t_{pd\pi}/\Delta_{pd}$ are *effective* covalency parameters for e_g, t_{2g} electrons, respectively, $d = eR_0$ is an elementary dipole moment for the cation-anion bond length R_0. We see that the local approximation results in an additional selection rule that forbids the $\sigma \rightarrow \pi$, and $\pi \rightarrow \sigma$ transitions $t_{1u}(\sigma) \rightarrow t_{2g}$, and $t_{1u,2u}(\pi) \rightarrow e_g$, respectively, though these transitions are dipole allowed. In other words, within the frame of this approximation, only σ-type $[t_{1u}(\sigma) \rightarrow e_g]$ or π-type $[t_{1u,2u}(\pi) \rightarrow t_{2g}]$ CT transitions are allowed. Hereafter, we use the terminology of "strong" and "weak" transitions for the dipole-allowed CT transitions which take place along the $\sigma-\sigma$, $\pi-\pi$ and $\pi-\sigma$, $\sigma-\pi$ channels, respectively. It should be emphasized that the local approximation, if nonzero, is believed to provide a leading contribution to the transition-matrix elements with corrections being on the first order in the cation-anion overlap integral. Moreover, the nonlocal terms are neglected in the conventional Hubbard-type approach. Equation (1) suggests extremely large dipole matrix elements and oscillator strengths for strong p-d CT transitions, mounting to $d_{ij} \sim e$Å and oscillator strength $f \sim 0.1$, respectively.

The conventional classification scheme of the CT transitions in the octahedral FeO_6^{9-} centers (intracenter CT transitions) incorporates the electric dipole-allowed transitions from the odd-parity oxygen $\gamma_u = t_{1u}(\pi), t_{2u}(\pi), t_{1u}(\sigma)$ orbitals to the even-parity iron $3dt_{2g}$ and $3de_g$ orbitals, respectively. These one-electron transitions generate the many-electron ones ${}^6A_{1g} \rightarrow {}^6T_{1u}$, which differ by the crystalline term of the respective $3d^{n+1}$ configuration,

$$(t_{2g}^3\, {}^4A_{2g}; e_g^2)\, {}^6A_{1g} \rightarrow [(t_{2g}^4; e_g^2)\, {}^5T_{2g}; \underline{\gamma_u}]\, {}^6T_{1u}, \qquad (2)$$

$$(t_{2g}^3\, {}^4A_{2g}; e_g^2)\, {}^6A_{1g} \rightarrow [(t_{2g}^3; e_g^3)\, {}^5E_g; \underline{\gamma_u}]\, {}^6T_{1u}, \qquad (3)$$

for $\gamma_u \rightarrow 3dt_{2g}$ and $\gamma_u \rightarrow 3de_g$ transitions, respectively. We see that in contrast to the manganese centers $[MnO_6]^{9-}$, each

one-electron $\gamma_u \rightarrow 3dt_{2g}$ transition generates one many-electron CT transition.[35]

Hence, starting with three nonbonding purely oxygen orbitals $t_{1u}(\pi), t_{1u}(\sigma), t_{2u}(\pi)$ as initial states for one-electron CT, we arrive at six many-electron dipole-allowed CT transitions ${}^6A_{1g} \rightarrow {}^6T_{1u}$. There are two transitions $t_{1u}(\pi), t_{2u}(\pi) \rightarrow t_{2g}$ ($\pi-\pi$ channel), two transitions $t_{1u}(\pi), t_{2u}(\pi) \rightarrow e_g$ ($\pi-\sigma$ channel), one transition $t_{1u}(\sigma) \rightarrow t_{2g}$ ($\sigma-\pi$ channel), and one transition $t_{1u}(\sigma) \rightarrow e_g$ ($\sigma-\sigma$ channel). In addition, one should account for a dipole-forbidden $t_{1g}(\pi) \rightarrow t_{2g}$ transition which determines the onset energy of the CT bands.

The formulas (1) allow us to make quantitative estimates for the relative magnitude of the intensities for different CT transitions. First of all, we would like to compare the overall integral intensities for the strong dipole-allowed CT transitions in the $\pi-\pi$ and $\sigma-\sigma$ channels. To this end, we calculate and sum the line strengths (the dipole-submatrix element squared) which are proportional to the appropriate oscillator strengths,

$$I_{\pi\pi} = 9\lambda_\pi^2 d^2; \quad I_{\sigma\sigma} = \frac{3}{2}\lambda_\sigma^2 d^2 \text{ or } I_{\pi\pi}/I_{\sigma\sigma} = 6\lambda_\pi^2/\lambda_\sigma^2. \quad (4)$$

In other words, the ratio of the total oscillator strengths for these channels is determined by the ratio of the respective cation-anion charge-density transfer parameters. Usually, $\lambda_\sigma^2 > \lambda_\pi^2$; however, it seems that the overall intensity for the $\pi-\pi$ channel can be comparable with that for the $\sigma-\sigma$ channel or can even exceed it.[35]

The transfer energy in the $Fe^{3+}O_6$ octahedra for the dipole-forbidden $t_{1g}(\pi)-t_{2g}$ transition which determines the onset energy of the p-d CT bands can be compared with a similar quantity for the dipole-forbidden $t_{1g}(\pi)-e_g$ transition which determines the onset energy of the p-d CT bands in $Mn^{3+}O_6$ octahedra in, e.g., manganite $LaMnO_3$,

$$\Delta^{\mathrm{Fe}}_{t_{1g}(\pi)-t_{2g}} - \Delta^{\mathrm{Mn}}_{t_{1g}(\pi)-e_g} = A + 28B - 10Dq - \Delta_{\mathrm{JT}} + I_3(\mathrm{Fe}) - I_3(\mathrm{Mn}).$$

Here we made use of standard Racah parameters, $I_3(\mathrm{Fe}), I_3(\mathrm{Mn})$ are the third ionization potentials for iron and manganese atoms, respectively, Δ_{JT} is the Jahn-Teller splitting of the e_g level in manganite. Given $A \approx 2.0$ eV (see below), $B \approx 0.1$ eV, $Dq \approx 0.1$ eV, $\Delta_{\mathrm{JT}} \approx 0.7$ eV, and $[I_3(\mathrm{Fe}) - I_3(\mathrm{Mn})] \approx -3.0$ eV (see, e.g., Ref. 36), we get $\Delta^{\mathrm{Fe}}_{t_{1g}(\pi)-t_{2g}} - \Delta^{\mathrm{Mn}}_{t_{1g}(\pi)-e_g} \approx 1.0$ eV. In other words, the onset of p-d CT transitions in the $Fe^{3+}O_6$ octahedra is expected to be noticeably ($\sim$1 eV) blueshifted as compared to its $Mn^{3+}O_6$ counterpart. Taking into account $\Delta^{\mathrm{Mn}}_{t_{1g}(\pi)-e_g} \approx 1.7$ eV as the onset energy of p-d CT transitions in the $Mn^{3+}O_6$ octahedra in an idealized orthomanganite $LaMnO_3$,[35] we get $\Delta^{\mathrm{Fe}}_{t_{1g}(\pi)-t_{2g}} \approx 2.7$ eV as an estimate of the onset energy of p-d CT transitions in the $Fe^{3+}O_6$ octahedra in the isostructural orthoferrite $LaFeO_3$. It is interesting that this low-energy p-d CT transition in ferrites can be superimposed on the d-d crystal-field transitions, in particular, on the ${}^6A_{1g} \rightarrow {}^4A_{1g}$ transition, which is usually an important optical signature of the Fe^{3+} centers. Indeed, its energy $\Delta E = 10B + 5C \approx 2.5$–$2.8$ eV does not depend on the crystal-field splitting parameter Dq that makes the energy of this transition insensitive to details of the crystalline surroundings. Quite to the contrary, both the energy and the intensity of the $t_{1g}(\pi)-t_{2g}$ p-d CT transition are strongly dependent on the crystalline surroundings. Being nominally dipole-forbidden for ideal $Fe^{3+}O_6$ octahedra, this transition becomes allowed for noncentrosymmetric $Fe^{3+}O_6$ complexes with a spectral weight typical for CT transitions. In contrast to the ${}^6A_{1g} \rightarrow {}^4A_{1g}$ transition, the low-symmetry distortions of $Fe^{3+}O_6$ octahedra give rise to a sizable splitting of the $t_{1g}(\pi)-t_{2g}$ band that may be used for the transition assignment.

As it was noted above, the onset energy for the p-d CT transitions in ferrites is blueshifted by 1 eV as compared to manganites. However, the low-energy strong dipole-allowed p-d CT transitions in ferrites and manganites are anticipated at $\sim$3 and $\sim$4.5 eV, respectively. Such a counterintuitive picture points to the importance of correlation effects governing the electronic structure in the ground and excited CT states.

B. Two-center d-d CT transitions

A two-center d-d CT transition in iron oxides with $Fe^{3+}O_6$ octahedra

$$[\mathrm{FeO_6}]^{9-} + [\mathrm{FeO_6}]^{9-} \rightarrow [\mathrm{FeO_6}]^{10-} + [\mathrm{FeO_6}]^{8-} \quad (5)$$

implies the creation of electron $[FeO_6]^{10-}$ and hole $[FeO_6]^{8-}$ centers with electron configurations formally related to Fe^{2+} and Fe^{4+} ions, respectively. Two-center d-d CT transitions from the initial $Fe^{3+}O_6(t_{2g}^3 e_g^2)$: ${}^6A_{1g}$ states can be directly assigned to $e_g \rightarrow e_g$, $e_g \rightarrow t_{2g}$, $t_{2g} \rightarrow e_g$, and $t_{2g} \rightarrow t_{2g}$ channels with final configurations and terms,

$$\begin{aligned} e_g &\rightarrow e_g: t_{2g}^3 e_g^1; {}^5E_g - t_{2g}^3 e_g^3; {}^5E_g, \\ e_g &\rightarrow t_{2g}: t_{2g}^3 e_g^1; {}^5E_g - t_{2g}^4 e_g^2; {}^5T_{2g}, \\ t_{2g} &\rightarrow e_g: t_{2g}^2 e_g^2; {}^5T_{2g} - t_{2g}^3 e_g^3; {}^5E_g, \\ t_{2g} &\rightarrow t_{2g}: t_{2g}^2 e_g^2; {}^5T_{2g} - t_{2g}^4 e_g^2; {}^5T_{2g}. \end{aligned} \quad (6)$$

In the framework of high-spin configurations, the $e_g \rightarrow t_{2g}$ CT transition has the lowest energy $\Delta = \Delta_{e_g - t_{2g}}$, while the $e_g \rightarrow e_g$, $t_{2g} \rightarrow t_{2g}$, and $t_{2g} \rightarrow e_g$ transitions have the energies $\Delta + 10Dq(3d^6)$, $\Delta + 10Dq(3d^4)$, and $\Delta + 10Dq(3d^6) + 10Dq(3d^4)$, respectively. The transfer energy in the Fe^{3+}-based ferrites for the $e_g \rightarrow t_{2g}$ CT transition

$$\Delta^{\mathrm{Fe\text{-}Fe}}_{e_g t_{2g}} = A + 28B - 10Dq$$

can be compared with a similar quantity for the $e_g \rightarrow e_g$ CT transition in Mn^{3+}-based manganite $LaMnO_3$

$$\Delta^{\mathrm{Mn\text{-}Mn}}_{e_g e_g} = A - 8B + \Delta_{\mathrm{JT}},$$

where Δ_{JT} is the Jahn-Teller splitting of the e_g levels in manganite. Given $B \approx 0.1$ eV, $Dq \approx 0.1$ eV, $\Delta_{\mathrm{JT}} \approx 0.7$ eV, and $\Delta^{\mathrm{Fe\text{-}Fe}}_{e_g e_g} \approx 2.0$ eV (see, e.g., Ref. 36), we get $A \approx 2.0$ eV, $\Delta^{\mathrm{Fe\text{-}Fe}}_{e_g t_{2g}} \approx 4.0$ eV. In other words, the onset of the d-d CT transitions in Fe^{3+}-based ferrites is strongly ($\sim$2 eV) blue-

shifted as compared to the Mn^{3+}-based manganite $LaMnO_3$.

1. Effect of orbital states and Me_1-O-Me_2 bond geometry

Another important difference between ferrites and manganites lies in the opposite orbital character of initial and final states for the d-d CT transitions. Indeed, the low-energy $d^4d^4 \rightarrow d^3d^5$ CT transition in manganites implies an orbitally degenerate Jahn-Teller initial state $^5E_g{}^5E_g$ and an orbitally nondegenerate final state $^4A_{2g}{}^6A_{1g}$, while the low-energy $d^5d^5 \rightarrow d^4d^6$ CT transitions in ferrites imply an orbitally nondegenerate initial state $^6A_{1g}{}^6A_{1g}$ and an orbitally degenerate Jahn-Teller final states such as $^5E_g{}^5E_g$ for $e_g \rightarrow e_g$ or $^5E_g{}^5T_{2g}$ for $e_g \rightarrow t_{2g}$ CT transitions. An unconventional final state with an orbital degeneracy on both sites or Jahn-Teller-excited states may be responsible for the complex multipeak line shape of the d-d CT band in ferrites.

The dipole-matrix element for the $\gamma_1 \rightarrow \gamma_2$ transition between the even-parity ground state Ψ^g_{GS} and the odd-parity excited state Ψ^u_{ES} of the Fe_A-Fe_B pair can be expressed through the transfer integral t_{12} and the transfer energy Δ_{12} as follows:

$$\langle \Psi^g_{\mathrm{GS}} | \hat{\mathbf{d}} | \Psi^u_{\mathrm{ES}} \rangle \approx 2e\mathbf{R}_{AB}\frac{t_{12}}{\Delta_{12}}. \tag{7}$$

In other words, the spectral weight of the two-center d-d CT transition can be related to the kinetic contribution $J_{\mathrm{kin}} = t_{12}^2/\Delta_{12}$ to the exchange integral in the AB pair.[36]

The transfer integrals in $3d$ oxides can strongly depend on the bond geometry. For two octahedral MeO_6 clusters sharing a common oxygen ion, we get the following expressions for the transfer integrals:

$$t_{12}(e_g0;e_g0) \approx t_{ss} + t_{\sigma\sigma}\cos\theta,$$

$$t_{12}(e_g0;e_g2) = t_{12}(e_g2;e_g0) = t_{12}(e_g2;e_g2) = 0,$$

$$t_{12}(e_g0;t_{2g}\mu) \approx t_{\sigma\pi}D^{(1)}_{0\mu}(\omega); \quad t_{12}(t_{2g}\mu;e_g0) \approx t_{\pi\sigma}D^{(1)}_{\mu 0}(\omega),$$

$$t_{12}(t_{2g}\mu_1;t_{2g}\mu_2) \approx t_{\pi\pi}D^{(1)}_{\mu_1\mu_2}(\omega), \tag{8}$$

where the $3d$ orbitals $e_g\mu(e_g0=d_{z^2}$, $e_g2=d_{x^2-y^2})$, $t_{2g}\mu$ $[t_{2g}\pm 1 = \mp\frac{1}{\sqrt{2}}(d_{xz} \pm id_{yz})$, $t_{2g}2=d_{xy}]$ are specified in the local coordinates for $Me(1)O_6$ and $Me(2)O_6$ clusters with z_1 and z_2 axes directed to the common oxygen ion; $t_{\alpha\beta}$ are transfer parameters for $\alpha(\beta)=s,\sigma,\pi$ bonds, respectively; θ is the Me(1)-O-Me(2) bond angle and $D^{(1)}_{\mu_1\mu_2}(\omega)$ is the Wigner rotation matrix[37] with ω being the Euler angles, specifying the transformation from the local coordinates for $Me(1)O_6$ to those for the $Me(2)O_6$ cluster. These expressions can be used to find a detailed relation between bond geometry and the spectral weight of the d-d CT transitions.

2. Spin dependence and temperature behavior

After uncovering the role of the Me-O-Me bond angle, we have to consider whether the spin degree of freedom affects the d-d CT transition. All the one-particle intersite transitions for the oxides with $3d$ cations obeying the Hund's rule can be divided into the so-called HS transitions $S_1S_2S \rightarrow S_1 \pm \frac{1}{2}S_2 \mp \frac{1}{2}S$ and the low-spin (LS) transitions $S_1S_2S \rightarrow S_1 - \frac{1}{2}S_2 - \frac{1}{2}S$. We note that despite the spinless character in the dipole moment operator, its matrix elements on the pair wave functions depend on the spin quantum numbers. In particular, the partial spectral weight (SW) for a $S_1S_2 \rightarrow S_1'S_2'$ transition can be given as follows:

$$\mathrm{SW}(S_1S_2 \rightarrow S_1'S_2') \propto [S_1,S_2'] \sum_S \rho_S \begin{Bmatrix} S_1 & S_2 & S \\ S_2' & S_1' & \frac{1}{2} \end{Bmatrix}^2, \tag{9}$$

where ρ_S is the temperature-dependent statistical weight of the S_1S_2S spin multiplet, and $\{\begin{smallmatrix} S_1 & S_2 & S \\ S_2' & S_1' & \frac{1}{2} \end{smallmatrix}\}$ is the $6j$ symbol.[37] Taking into account the expressions for $6j$ symbols, we see that the temperature dependence of the partial spectral weight $\mathrm{SW}(S_1S_2 \rightarrow S_1'S_2')$ should be determined by a statistical average $\langle S(S+1)\rangle = \langle \hat{\mathbf{S}}^2 \rangle$ which, in its turn, relates to the spin-spin-correlation function $\langle (\hat{\mathbf{S}}_1 \cdot \hat{\mathbf{S}}_2) \rangle$. Thus, we should conclude that the partial spectral weight for $S_1S_2S \rightarrow S_1'S_2'S$ transitions in an isolated spin pair is governed by a spin-dependent prefactor containing the spin-spin-correlation function $\langle (\hat{\mathbf{S}}_1 \cdot \hat{\mathbf{S}}_2) \rangle$. For the HS transition $S_1S_1 \rightarrow S_1 - \frac{1}{2}S_1 + \frac{1}{2}$ and the LS transition $S_1S_1 \rightarrow S_1 - \frac{1}{2}S_1 - \frac{1}{2}$ in the pair of identical $3d$ ions, one gets

$$\mathrm{SW}\left(S_1S_1 \rightarrow S_1 - \frac{1}{2}S_1 + \frac{1}{2}\right) \propto \frac{\langle S(S+1)\rangle}{2S_1(2S_1+1)} = \frac{[\langle (\hat{\mathbf{S}}_1 \cdot \hat{\mathbf{S}}_2)\rangle + S_1(S_1+1)]}{S_1(2S_1+1)}, \tag{10}$$

$$\mathrm{SW}\left(S_1S_1 \rightarrow S_1 - \frac{1}{2}S_1 - \frac{1}{2}\right) \propto \frac{[2S_1(2S_1+1) - \langle S(S+1)\rangle]}{2S_1(2S_1+1)} = \frac{[S_1^2 - \langle (\hat{\mathbf{S}}_1 \cdot \hat{\mathbf{S}}_2)\rangle]}{S_1(2S_1+1)}, \tag{11}$$

respectively. These expressions allow one to obtain both the low-temperature ($T \ll T_N$) and high-temperature [$T \gg T_N$, $\langle \hat{\mathbf{S}}_i \cdot \hat{\mathbf{S}}_j \rangle \rightarrow 0$] limits for the spin prefactor. In accordance with a spin sum rule, the sum of spin prefactors on the right-hand sides of the expressions (10) and (11) turns into unity due to the exact compensation of temperature-dependent terms with the spin-spin-correlation function. In other words, the higher-energy LS bands exhibit a strictly inverse SW evolution with temperature as compared to the HS band. Varying the temperature, we get the SW transfer between the HS and the LS subbands. It should be noted that for the Fe^{3+} ion-based oxides we deal only with the LS transitions $\frac{5}{2}\frac{5}{2} \rightarrow 22$ and the antiferromagnetic ground-state exchange coupling.

C. Electron-lattice polarization effects, self-trapping of CT excitons, and unstable CT insulators

The relaxation of optically excited CT states can strongly affect both the optical response and the main physical properties of the insulator. The CT relaxation is governed by a cumulative effect of *electronic* and *ionic* terms associated

with the displacement of electron shells and ionic cores, respectively.[38] The former term is due to the *nonretarded* effect of the electronic polarization by the momentarily localized electron-hole (EH) pair, with the ionic cores fixed at their undisturbed crystallographic positions. Such a situation is typical for the lattice response accompanying Franck-Condon transitions (optical excitation and photoionization). On the other hand, all the long-lived excitations, i.e., all the intrinsic thermally activated states and the extrinsic particles produced as a result of doping, injection, or optical pumping, should be regarded as stationary states of a system with a deformed lattice structure. These relaxed states should be determined from the condition that the energy of the system has a local minimum when the interaction of the electrons and holes with the lattice deformations is taken into account. This means that we cannot, strictly speaking, make use of the same energy parameters to describe the optical (e.g., photoexcited) and the thermal (e.g., doped) holes.

The lattice relaxation energies $-\Delta R_{\mathrm{th}}$ associated with the hole/electron localization in $3d$ oxides are particularly large. For instance, in $LaMnO_3$ the optical (nonrelaxed) energies of the creation of a hole on Mn and O sites are 2.6 and 4.9 eV, respectively, while $-\Delta R_{\mathrm{th}}^{\mathrm{Mn}}=0.7-0.8$ and $-\Delta R_{\mathrm{th}}^{\mathrm{O}}=2.4$ eV.[39] In other words, the electronic hole is more stable at the Mn site than at the O site in the $LaMnO_3$ lattice; however, both possibilities should be treated seriously.

Shell-model estimates[39] yield for the energy of the optically excited electron-hole formation $E_{\mathrm{opt}}\approx 3.7$ eV in the parent manganite $LaMnO_3$, while the respective thermal relaxation energy is estimated as $-\Delta R_{\mathrm{th}}\approx 1.0$ eV. Such an estimate seems to be typical for different insulators.[38] In any case, we deal with a several eV effect both for electronic and ionic contributions to the relaxation energy.

Figures 2(a) and 2(b) illustrate two possible ways by which the electron-lattice polarization governs the CT exciton evolution. Shown are the adiabatic potentials (APs) for the two-center ground-state configuration and the excited CT configuration. Coordinate Q is associated with a lattice degree of freedom. For the lower branch of the AP in the system, we have either a single minimum point for the ground-state configuration [Fig. 2(a)] or a two-well structure with an additional local minimum point [Fig. 2(b)] associated with the self-trapped CT exciton.[40] This "bistability" effect is of primary importance for our analysis. Indeed, these two minima are related to two (meta)stable charge states with and without CT, respectively, which form two candidates to compete for the ground state. It is worth noting that the self-trapped CT exciton may be described as a configuration with a negative correlation energy U. Thus, one can conclude that all systems such as $3d$ oxides may be divided into two classes: *CT stable systems* with only the lower AP branch minimum for a certain charge configuration and bistable or *CT unstable systems* with two lower AP branch minima for two local charge configurations; one of which is associated with the self-trapped CT excitons resulting from the self-consistent charge transfer and electron-lattice relaxation.[38]

Two-center CT excitons have a very large fluctuating electric dipole moment $|d|\sim 2eR_{\mathrm{MM}}$ and therefore can be involved into an attractive electrostatic dipole-dipole interaction. This is believed to be an important incentive to the proliferation of excitons and formation of excitonic clusters. The CT excitons are proved to attract and form molecules called biexcitons, and more complex clusters where the individuality of the separate exciton is likely to be lost. Moreover, one may assume that like in semiconductors with an indirect-band gap, it is energetically favorable for the system to separate into a low-density exciton phase coexisting with microregions of a high-density two-component phase composed of electron and hole centers or EH droplets. Indeed, the excitons may be considered to be well-defined entities only at small concentrations, whereas at large densities their coupling is screened and their overlap becomes so considerable that they loose individuality and we arrive at a system of electron and hole centers, which form an electron-hole Bose liquid.[41]

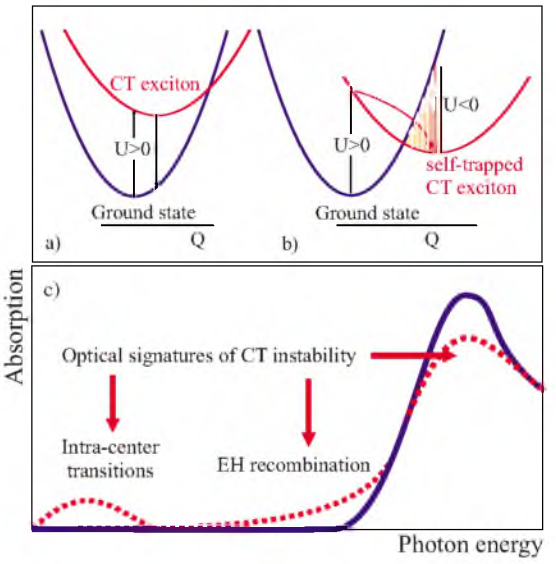

FIG. 2. (Color online) Simple illustration of the electron-lattice polarization effects for CT excitons (see text for details): (a) GS configuration and (b) two-well structure. (c) Optical response (schematically) of the self-trapped CT excitons and EH droplets (dotted curves). Arrows point to a spectral weight transfer from the bare CT band to the CT gap with an appearance of midgap bands and/or smearing of the fundamental absorption edge.

An increase in injected excitons in this case merely increases the size in the EH droplets, without changing the free exciton density. However, the level of intrinsic nonstoichiometry in $3d$ oxides is significant (one charged defect per 100–1000 molecular units is common). The charged defect produces a random electric field, which can be very large (up to 10^8 V cm^{-1}; $\sim$ a field at nuclei) thus promoting the condensation of CT excitons and the *inhomogeneous nucleation* of EH droplets.

The CT unstable systems will be characterized by a well-developed volume fraction of short- and long-lived CT excitons or EH droplets that can give rise to a specific optical response in a wide spectral range due to various p-d and d-d CT transitions. First, these are the p-d CT transitions in electron and hole centers and the inverse d-d CT transitions or EH recombination processes (see Fig. 2). Their spectral weight can be easily revealed in the spectral window of the bare insulator to be a direct indicator of the CT instability.

Figure 2(c) illustrates main features of the optical response for the CT unstable insulators, that is, the spectral weight transfer from the bare CT band to the CT gap with an appearance of the midgap bands and/or smearing of the fundamental absorption edge.

Concluding this section, we should point to an unusually large electric polarizability of the two-center *d-d* CT excitons that makes the self-trapped excitons potentially important contributors to the magnetoelectric performance.

III. EXPERIMENTAL

We have performed an optical study of bismuth ferrite $BiFeO_3$ and several other iron oxides. One group includes oxides with only octahedral Fe^{3+} centers. These are $BiFeO_3$, the orthoferrites $ErFeO_3$, $Y_{.95}Bi_{.05}FeO_3$, hematite α-Fe_2O_3, gallium ferrite with the hematite structure $Fe_{2-x}Ga_xO_3$, and the orthorhombic iron borate Fe_3BO_6. The second group includes oxides with octahedral and tetrahedral Fe^{3+} centers. These are the calcium ferrite $Ca_2Fe_2O_5$ with the brownmillerite structure, the model lithium ferrite $LiFe_5O_8$ with the spinel structure, the samarium-iron oxide $Sm_3Fe_5O_{12}$ with the garnet structure, and uniaxial hexaferrite $BaFe_{12}O_{19}$ with the magnetoplumbite structure.

Samples in the form of x-ray-oriented plane-parallel Syton-polished platelets were prepared from single crystals grown by the flux method. Orthoferrites were grown by the floating-zone method.[42]

Some previously reported optical data on ferrites were in most cases obtained with the use of conventional reflection and absorption methods. We performed our study using a variable-angle spectroscopic ellipsometer as described elsewhere.[43,44] The technique of optical ellipsometry provides significant advantages over conventional reflection and transmittance methods in that it is self-normalizing and does not require reference measurements. The optical complex pseudodielectric function $\varepsilon=\varepsilon'-i\varepsilon''$ is obtained directly without a Kramers-Krönig transformation. From the measured ellipsometric angles ψ and Δ, we calculated the pseudodielectric function

$$\varepsilon^{ps}=\sin^2\theta\left[1+\tan^2\theta\left(\frac{1-\rho}{1+\rho}\right)^2\right], \tag{12}$$

where $\rho=\tan\psi e^{i\Delta}$ and θ is the angle of incidence.[45] For an isotropic crystal, this function gives the value of the dielectric function of the material $\varepsilon=\varepsilon^{ps}$ if a surface roughness is taken into account properly. In the case of uniaxial crystals,[46,47] the pseudodielectric function extracted from the measurements performed for two different orientations of the sample are a good approximation for the true dielectric function of the crystal. Thus, ε^{ps} measured with *p*-polarized light for a crystal with the optical axis *z* lying in the plane of incidence gives the value of ε_{zz} and, subsequently, of the extraordinary refractive and absorption indices. The value for $\varepsilon_{xx}=\varepsilon_{yy}$ and the ordinary refractive and absorption indices can be obtained in the same way when the optical axis is perpendicular to the plane of incidence.

In the case of biaxial crystal, the pseudodielectric function (12) can be again a reasonable approximation, if the sample is properly oriented with one of the principle directions being perpendicular to the sample surface. In this case, ε^{ps} is comprised by the projections of the components of dielectric tensor along the two principle directions lying in the plane of incidence.[46] Thus, for the large angles of incidence used in our experiments ($\theta=60°-72°$), the spectral behavior of ε^{ps} represents mainly the spectral behavior of the dielectric function for light polarized along the direction parallel to the intersection of the sample surface and the plane of incidence. Thus, performing the ellipsometric measurements from different surfaces of the crystal, information of the spectral features of the dielectric function along all three principle directions of the crystal can be obtained. We note that a more comprehensive treatment of the ellipsometric data[46] will result in small corrections of the absolute values of the dielectric functions, without significant effect on the main spectral features.

This approximation, strictly speaking, is valid for large values of $|\varepsilon|$, i.e., in the range of strong absorption. In the low absorption range, however, the optical anisotropy is usually not resolved in ellipsometric measurements. Therefore, the pseudodielectric function can be used as an approximation for a dielectric function in the low absorption range.

Surface roughness and depolarization effects affect mostly the results in the low absorption range but not the positions and the strength of intensive absorption bands. We note that for all samples considered here, the measurements were performed for several large angles of incidence θ. The coincidence of the dielectric functions extracted from these measurements points to the validity of the approach used.

The dielectric function ε was obtained in the range from 0.6 to 5.8 eV. The comparative analysis of the spectral behavior of ε_1 and ε_2 is believed to provide a more reliable assignment of the spectral features as compared to reflectivity measurements. The spectra were analyzed using the set of Lorentz functions,

$$\varepsilon=\varepsilon'-i\varepsilon''=\varepsilon_0+\sum\frac{f_j}{E_{0j}^2-E^2-iE\Gamma_j}, \tag{13}$$

where f_j characterizes the strength of the *j*th oscillator with a central frequency E_{0j} and a half width Γ_j, ε_0 is the dielectric susceptibility at $E=0$.

A. Experimental data

1. Fe^{3+} ions in octahedral positions

Bismuth ferrite $BiFeO_3$. In the bulk form, $BiFeO_3$ has a rhombohedrally distorted cubic perovskite cell and belongs to the $R3c$ space group.[48–50] Iron Fe^{3+} ions occupy noncentrosymmetric positions $6c$ with three short (1.952 Å) and three long (2.105 Å) Fe-O bonds. Fe^{3+} ions are shifted along the threefold axis by about 0.134 Å from the center of the oxygen octahedra. Along with this, two different Bi-Fe distances about 3.06 and 3.87 Å along the threefold axis are supposed to be the origin of the ferroelectricity in $BiFeO_3$.[49,50] The antiferromagnetic ordering temperature $T_N=643$ K and the ferroelectric temperature $T_c=1143$ K.[48]

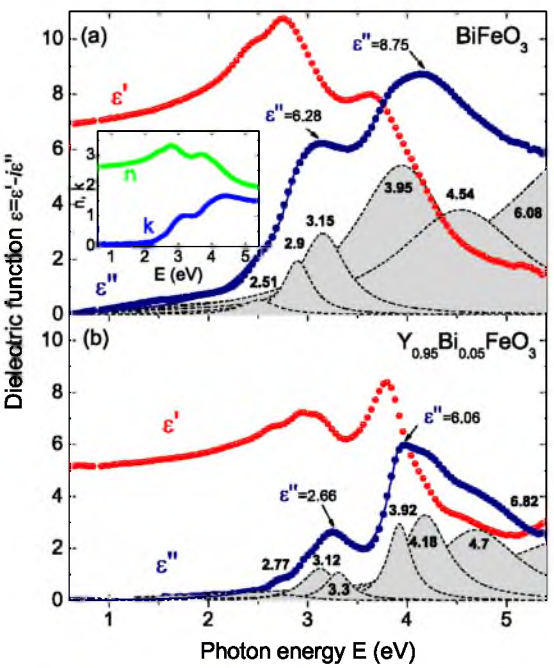

FIG. 3. (Color online) (a) The dielectric functions and the contributing modes in $BiFeO_3$. Inset shows indices of absorption and refraction. (b) The dielectric function in orthoferrite $Y_{.95}Bi_{.05}FeO_3$.

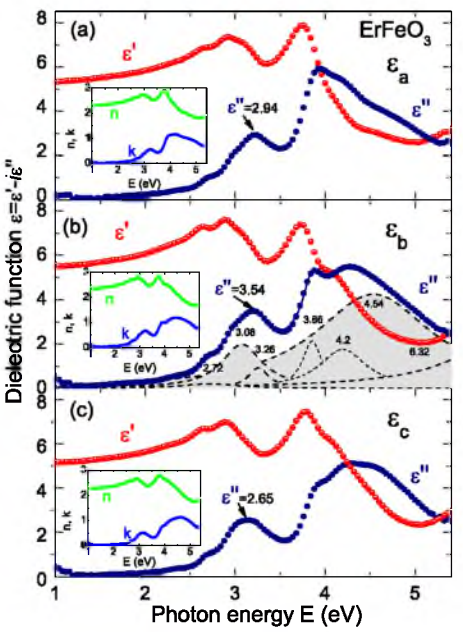

FIG. 4. (Color online) The dielectric function spectra in $ErFeO_3$ orthoferrite for three main polarizations. Insets show indices of absorption and refraction. Note that the region below 1 eV is not shown because of strong interference effects, which occur due to the high transparency of the samples in this region.

Recent reports suggest orientation phase transitions below room temperature[51] similar to those in orthoferrites.[52]

The ellipsometric measurements were done from the polished (001)-type surface with incident light polarizations along the [110], [1$\bar{1}$0], and [100] directions. We observed optical anisotropy in the range of several percent, but since the sample studied was most probably in a multidomain ferroelectric state we do not discuss it in this paper. We note that strong optical birefringence in $BiFeO_3$ was also reported in Ref. 53. Figure 3(a) shows the $\varepsilon', \varepsilon''$ spectra of $BiFeO_3$. Inset in Fig. 3(a) shows the indices of absorption k and refraction n. Two groups of strong CT transitions are clearly seen around 3.0 and 4.0 eV. It is worth noting the enhanced structureless spectral weight in a wide range below the main CT bands with a remarkable smearing of the fundamental edge. The ε_2 value at 2.0 eV amounts almost to $\varepsilon_2 = 1.0$ which is an order of magnitude larger than in many other ferrites.

Orthoferrites. Orthoferrites $ErFeO_3$ and $Y_{.95}Bi_{.05}FeO_3$ belong to the distorted perovskitelike structure with the space group *Pbnm*.[52] There are four Fe^{3+} ions in the unit cell in the centrosymmetric octahedral positions 4*b*. The Néel temperature lies in the range of 650 K. The $\varepsilon', \varepsilon''$ spectra of $ErFeO_3$ for three main polarizations shown in Fig. 4 are typical for the known spectra of orthoferrites $RFeO_3$.[33,44] Two groups of intense bands are distinguished around 3.0 and 4.0 eV.

Spectra of orthoferrites differ from those of $BiFeO_3$ where the main bands are noticeably more intense, in particular, the low-energy 3 eV band. This is well demonstrated by Fig. 3 where the optical spectra of the two perovskites $BiFeO_3$ and $Y_{.95}Bi_{.05}FeO_3$ are compared. At the same time we see in Fig. 3(b) that 5% substitution of Y for Bi does not produce any noticeable changes in the spectra of orthoferrites.

Hematite α-Fe_2O_3. The hematite α-Fe_2O_3 is an iron oxide with the highest concentration of Fe^{3+} ions. The crystal structure is described by a rhombohedral space group $R\bar{3}c$. As in $BiFeO_3$, the Fe^{3+} ions occupy noncentrosymmetric positions 12*c* with three short (1.944 Å) and three long (2.113 Å) Fe-O bonds.[54,55] The Fe^{3+} ions are shifted along the threefold axis from the center of the oxygen octahedra. Each FeO_6 octahedron shares a face with another one in the layer above or below. High concentration and strong coupling between Fe^{3+} ions via oxygen ions leads to the high Néel transition temperature $T_N = 948$ K. Below this temperature α-Fe_2O_3 is piezomagnetic. Figure 5(a) shows optical dielectric spectra of hematite for the incident light polarization in the basal plane.

The dielectric spectra for two principal polarizations in gallium-substituted hematite α-$Fe_{2-x}Ga_xO_3$ are shown in Figs. 5(b) and 5(c). This material with $x = 0.25$ has the same trigonal crystal structure as hematite. General spectral features of the two materials are similar. However, despite the noticeable dilution of the iron sublattice, the integral intensity of the CT bands reveals a noticeable rise rather than the expected reduction.

Iron borate Fe_3BO_6. This material crystallizes in an orthorhombic-type structure.[56–58] The space group is *Pnma* with 4 f.u. per unit cell. The iron Fe^{3+} ions are located on two nonequivalent 4*c* and 8*d* sites. Both crystallographically independent iron ions are octahedrally coordinated by six oxygen O^{2-} ions. Both positions are strongly distorted in comparison to other ferrites. For one sublattice, the Fe-O bond length varies from 1.865 to 2.226 Å, for the second sublattice from 1.905 to 2.131 Å. Iron ions form antiparallel spin arrangements within and between sublattices and Fe_3BO_6 is

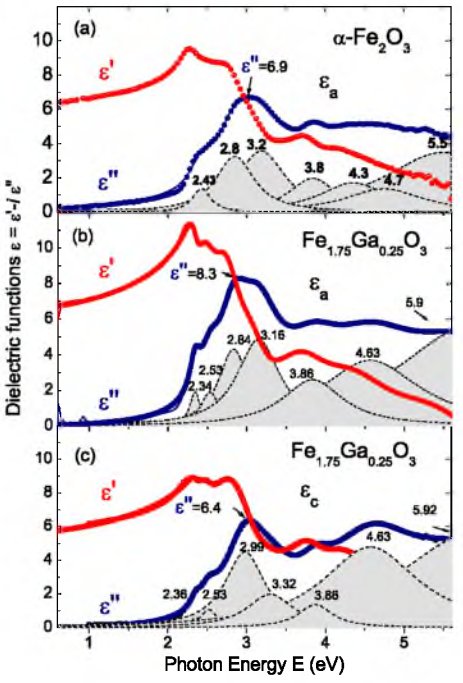

FIG. 5. (Color online) The dielectric function spectra of hematite α-Fe_2O_3 (a) and gallium-substituted hematite α-$Fe_{2-x}Ga_xO_3$ with [(b) and (c)] $x=0.25$.

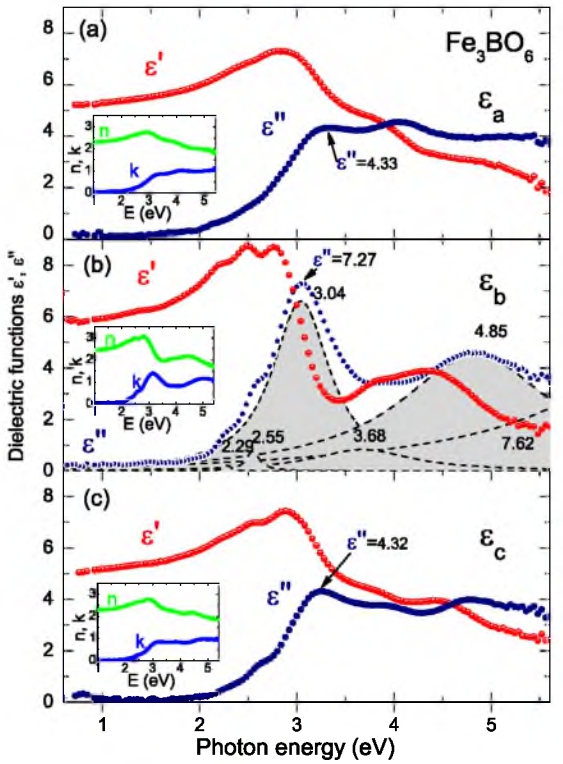

FIG. 6. (Color online) The dielectric function spectra of Fe_3BO_6 for the three main polarizations. Insets show indices of absorption and refraction.

an antiferromagnet below $T_N=508$ K and a canted antiferromagnet below $T_c=430$ K.[58]

Dielectric spectra for three main polarizations are shown in Figs. 6(a)–6(c). The strongest band at 3.06 eV is observed in the *b* polarization. In its general features, the spectrum for this polarization looks similar to the hematite spectrum [see Fig. 5(a)]. The CT spectra for the *a* and *c* polarizations are less intense and resemble one another, whereas the 3.06 eV band is suppressed. The observed strong trichroism was related to the low symmetry on both iron sites.[59] We note that the Fe_3BO_6 spectra radically differ from the known spectra of other iron borates. Optical transitions in Fe_3BO_6 are noticeably more intense and the band gap is redshifted in comparison to other borates, $FeBO_3$ ($T_N=348$ K) and $GdFe_3(BO_4)_3$ ($T_N=37$ K).[60,61] In contrast to Fe_3BO_6, these borates are highly transparent in the visible spectral range; the charge transfer bands are less intense and are shifted to higher photon energy. The most plausible explanation of these differences can be related to the iron/oxigen ratio which varies in these three compounds as 1/2, 1/3, and 1/4, respectively.

2. Fe^{3+} ions in octahedral and tetrahedral positions

All materials we discussed above contain magnetic Fe^{3+} ions only in octahedral positions. From a magnetic point of view, they are antiferromagnets or, more strictly speaking, weak ferromagnets due to the canting of the antiferromagnetic sublattices derived from the Dzyaloshinsky-Moriya coupling and single-ion anisotropy. The materials we discuss below contain Fe^{3+} ions in octahedrally and tetrahedrally coordinated positions. Calcium ferrite is an antiferromagnet, whereas all other materials are ferrimagnets due to the nonequivalency of the magnetic ions in the two types of positions. Our main goal is to elucidate the relative contribution to the optical response of the tetrahedral Fe^{3+} centers. To this end, we address a series of ferrites with a rising fraction of tetrahedral Fe^{3+} centers.

Lithium ferrite $LiFe_5O_8$. Lithium ferrite $LiFe_5O_8$ has the cubic spinel structure, the space group $P4_332$ is noncentrosymmetric due to the one-to-three ordering of the Li and Fe ions on the octahedral sites.[55,62] The Fe^{3+} ions occupy the octahedral and tetrahedral crystallographic sites with a ratio of 4:1. Lithium ferrite has one of the highest ferrimagnetic-paramagnetic transition temperature $T_c=943$ K which is remarkably close to that of hematite.[55] $LiFe_5O_8$ is a material in which the linear magnetoelectric effect was reported.[10] A spontaneous nonreciprocal circular dichroism was observed in Ref. 11. Lithium ferrite is a promising candidate for multilayered ferrimagnetic-ferroelectric composites exhibiting a large microwave magnetoelectric susceptibility.[63] Figure 7(a) shows the dielectric functions measured on a polished (110) plate. It is worth noting that the optical spectra of $LiFe_5O_8$ resemble those of hematite. It points to a predominant contribution of the octahedral Fe^{3+} centers to optical transitions. The well-pronounced spectral features at 2.4 and 2.56 eV coincide with those observed in the spectral dependencies of the circular dichroism[11] and linear Kerr effect.[64] They are assigned to the *d-d* transitions in the Fe^{3+} ions in the octahedral and tetrahedral positions, respectively. The high intensity of the 2.56 eV transition ($\varepsilon''=3.8$) should be noted.

Hexaferrite $BaFe_{12}O_{19}$. Hexaferrites are a very large group of ferrimagnetic materials with a hexagonal structure

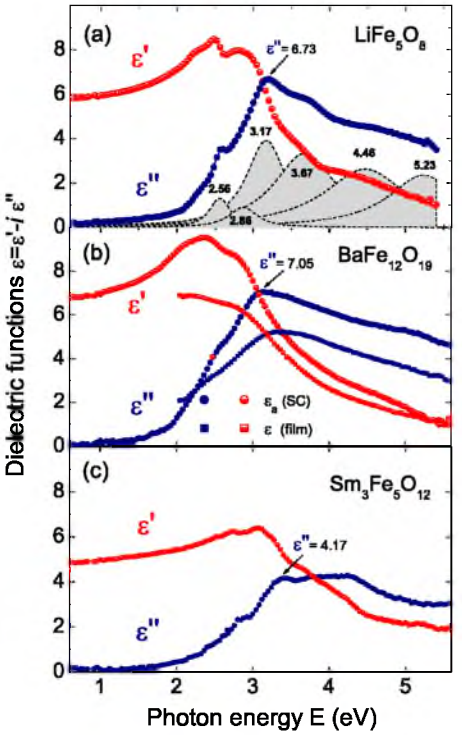

FIG. 7. (Color online) The dielectric function spectra of several ferrites with octahedral and tetrahedral Fe^{3+} centers: (a) lithium ferrite $LiFe_5O_8$, (b) hexaferrite $BaFe_{12}O_{19}$, and (c) rare-earth garnet $Sm_3Fe_5O_{12}$. For $BaFe_{12}O_{19}$, spectra of ε' were measured for a single crystal and a polycrystalline thin film (film).

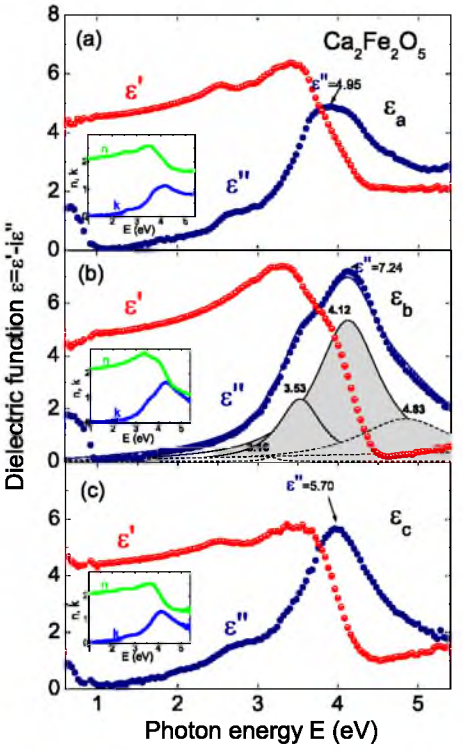

FIG. 8. (Color online) The dielectric function spectra in calcium ferrite $Ca_2Fe_2O_5$ for three main polarizations. Insets show indices of absorption and refraction.

where Fe^{3+} ions occupy slightly distorted octahedral and tetrahedral positions. For a review of their properties, see Ref. 65. In barium hexaferrite $BaFe_{12}O_{19}$ (magnetoplumbite), the Fe^{3+} ions occupy nine octahedral, two tetrahedral, and one new fivefold positions. The experimental optical spectra for the (0001) face of a single crystal and a thin ($\sim 1\mu$) polycrystalline film are shown in Fig. 7(b). Predominance of the octahedral positions makes the optical response in $BaFe_{12}O_{19}$ similar to that of $LiFe_5O_8$ and hematite.

Rare-earth garnet $Sm_3Fe_5O_{12}$. Garnets possess the cubic structure *Ia*3*d* with 8 f.u. in the unit cell. Fe^{3+} ions occupy slightly distorted octahedral 24*c* positions and tetrahedral 16*a* positions with a ratio of 3:2. Review of crystallographic and physical properties of magnetic garnets can be found in Refs. 66 and 67. Iron garnets are ferrimagnetic and the ordering temperature of iron sublattices are in the range of about 550 K. Experimental spectra of dielectric functions are shown in Fig. 7(c). In general features, they are similar, but not exactly the same, as those reported in Refs. 68 and 69.

Calcium ferrite $Ca_2Fe_2O_5$. This ferrite crystallizes in the orthorhombic space group of the brownmillerite-type *Pnma*.[70,71] The Fe^{3+} ions occupy the octahedral 4*a* and tetrahedral 4*c* crystallographic sites with a ratio of 1:1. The Fe-O distances in the octahedral positions are 1.963 Å ($4O^{2-}$) and 1.977 Å ($2O^{2-}$). For the tetrahedral sites, these are 1.884 ($2O^{2-}$), 1.858, and 1.859 Å. These data show that both positions are only slightly distorted, e.g., compare them with data given above for the iron borate. Calcium ferrite is an antiferromagnet with T_N=725 K (see Refs. 48 and 72 and references therein). The dielectric spectra in the calcium ferrite for three principal polarizations are shown in Figs. 8(a)–8(c). At first sight, in $Ca_2Fe_2O_5$ with the same content of octahedral and tetrahedral centers, one should expect a competition of comparable contributions of the CT transitions related with octahedral and tetrahedral Fe^{3+} centers. However, we see that the spectra differ from all the spectra discussed above, in particular, from those of lithium ferrite and magnetoplumbite where iron ions are also in octahedral and tetrahedral positions. Unexpectedly, we observe a very strong CT-like band peaked near 0.5 eV that was not reported earlier. The 3.0 eV band, a visiting card of octahedral Fe^{3+} centers, is strongly suppressed due to a puzzling spectral weight transfer to the midinfrared range. The spectra of $Ca_2Fe_2O_5$ for *a* and *c* polarizations are less intense, resemble one another, but are not identical. Pronounced optical anisotropy could be related to the crystallographic features of $Ca_2Fe_2O_5$ having a pseudoquadratic layered structure (see Figs. 2 and 3 in Ref. 71). We note that magnetic structure of $Ca_2Fe_2O_5$ is still a matter of debate.[72–74]

IV. DISCUSSION

To begin our discussion of the CT transitions in different ferrites, we refer to the spectroscopic data for garnets $Y_3Fe_xGa_{5-x}O_{12}$ (x=5,3.9,0.29,0.09).[68] They demonstrate that the optical response in the spectral range up to 30 000 cm^{-1} (~3.7 eV) is governed by the on-center transitions for both octahedral and tetrahedral Fe^{3+} centers. It means that the onset energy for different *d*-*d* CT transitions

in ferrites is expected to be >3.7 eV in agreement with our model estimates discussed in Sec. II.

To uncover the role played by the octahedral Fe^{3+} centers, we turn to the optical response of the orthoferrites $RFeO_3$. These compounds contain the only type of centrosymmetric, slightly ($\sim 1\%$) distorted, FeO_6 octahedra. Despite the long story of optical and magneto-optical studies (see, e.g., Refs. 33 and 75), the microscopic origin of the main spectral features in orthoferrites remains questionable and the transition assignments made earlier in Ref. 33 need a comprehensive revisit. The spectra of $ErFeO_3$ for three main polarizations shown in Fig. 4 are typical for orthoferrites $RFeO_3$.[33,44,75] The low-energy intense band around 3 eV may be assigned to a strong dipole-allowed on-center $t_{2u}(\pi) \rightarrow t_{2g}$ CT transition as was proposed in Ref. 33. This is a characteristic feature of the octahedral Fe^{3+} centers in oxides, with the calcium ferrite being a puzzling exception. However, such an assignment also implies the existence of a weak band due to a low-energy dipole-forbidden on-center $t_{1g}(\pi) \rightarrow t_{2g}$ CT transition redshifted by about 0.8 eV as expected from estimates.[34] Indeed, a band around 2.5 eV is found in the optical and magneto-optical spectra of different orthoferrites.[33] This band is clearly visible in hematite α-Fe_2O_3 near 2.4 eV (see Fig. 5), where the $t_{1g}(\pi) \rightarrow t_{2g}$ transition becomes allowed due to a breaking of the centrosymmetry for Fe^{3+} centers.

The nearest high-energy neighborhood of the 3 eV band is expected to be composed of $t_{1u}(\pi) \rightarrow t_{2g}$ CT transitions with a comparable intensity and estimated energy about 4 eV. All the dipole-allowed on-center p-d CT transitions to the e_g state are blueshifted by $10Dq(3d^5)$ as compared to their $\gamma \rightarrow t_{2g}$ counterparts with the onset energy on the order of 4 eV. Interestingly, for the dipole-allowed $\gamma_u \rightarrow t_{2g}$ transitions, the maximum intensity is expected for the low-energy $t_{2u}(\pi) \rightarrow t_{2g}$ transition, while for $\gamma_u \rightarrow e_g$ transitions the maximum intensity is expected for the high-energy ($\sim 6-7$ eV) $t_{1u}(\sigma) \rightarrow e_g$ transition. The analysis of the experimental spectra of orthoferrites demonstrates the failure of the on-center p-d CT transitions to explain the broad intensive band centered near 4.5 eV together with a narrow low-energy satellite peaked near 3.9 eV. Both features are typical for orthoferrites[33,75] and may be assigned to a $e_g \rightarrow t_{2g}$ low-energy two-center CT transition ${}^6A_{1g}\,{}^6A_{1g} \rightarrow {}^5E_g\,{}^5T_{2g}$ to an unconventional final state with an orbital degeneracy on both sites. These Jahn-Teller-excited states are responsible for the complex line shape of the $e_g \rightarrow t_{2g}$ CT band which is composed of a narrow excitonlike feature and a broad intense band separated by ~ 0.5 eV, which is believed to be a measure of the Jahn-Teller splitting in the excited state. Thus, we see that all the spectral features observed in the optical spectra of orthoferrites for energies below 5 eV can be directly assigned to the low-energy p-d and d-d CT transitions.

It is worth noting that the dielectric function in orthoferrites is nearly isotropic due to very weak ($\sim 1\%$) rhombic distortions of FeO_6 octahedra and nearly equivalent different Fe-O-Fe bonds. Nevertheless, a fine structure of the main CT bands is clearly revealed in magneto-optical spectra of orthoferrites, which was assigned to the dipole-forbidden d-d crystal-field transitions.[33,75] In our opinion, their relation to the low-symmetry distortions in the p-d CT band seems to be more reasonable.

The effect of a strong change in bulk crystalline symmetry and local trigonal noncentrosymmetric distortions of FeO_6 octahedra is well illustrated by the optical response of hematite α-Fe_2O_3. First of all, there is a noticeable rise of intensity and a splitting for dipole-forbidden $t_{1g}(\pi) \rightarrow t_{2g}$ transition at 2.4 eV, which is clearly visible in the spectra of the gallium-substituted sample [Figs. 5(b) and 5(c)]. Second, one should note a clear splitting on the order of 0.3–0.4 eV of the 3 eV band due to a sizable trigonal distortion of the FeO_6 octahedra. In both cases, the band splitting effect reflects the singlet-doublet splitting of the initial orbital triplets $t_{1g}(\pi)$ and $t_{2u}(\pi)$, respectively, due to the low-symmetry trigonal crystal field. Interestingly, the integral intensity of the $t_{2u}(\pi) \rightarrow t_{2g}$ band at 3 eV is visibly enhanced in hematite as compared to similar bands in orthoferrites that may result from the more covalent Fe-O bonding in hematite. Such an explanation agrees with the increase in the Fe-O-Fe exchange coupling and higher values of T_N.

Comparing the optical response for both orthorhombic ferrites $ErFeO_3$ and $Y_{.95}Bi_{.05}FeO_3$, we see that the 5% substitution of rare-earth ion (or Y) for Bi does not produce any noticeable changes in the spectra of orthoferrites. However, the optical spectrum of rhombohedral $BiFeO_3$ differs significantly from that of orthorhombic orthoferrites in several points. It mostly resembles that of rhombohedral hematite α-Fe_2O_3 with an additional broad intense band centered near 4 eV, which may be assigned to CT transitions in the Bi-O sublattice. The close relation with the hematite spectra is a direct result of the close similarity in the rhombohedral and noncentrosymmetric distortions of the FeO_6 octahedra in both compounds. It is worth noting that the Lorentzian fitting distinctly points to a small shoulder centered at 2.5 eV. This feature can be unambiguously attributed to the dipole-forbidden $t_{1g}(\pi) \rightarrow t_{2g}$ CT transition similar to other ferrites with FeO_6 centers. Such a feature was observed in earlier studies,[20,22] however, without any explanation. Most recent absorption and cathodoluminescence spectra[27] reveal a fine three-peak structure of the 2.5 eV band in full accordance with low-symmetry (monoclinic) distortions of the epitaxial thin films. The authors attributed this to defect states due to oxygen vacancies; however, we see its intrinsic nature related to a low-lying $t_{1g}(\pi) \rightarrow t_{2g}$ CT transition typical for all the ferrites with octahedral FeO_6 centers.

The calculations of the electronic structure of $BiFeO_3$ within the LSDA, LSDA+U,[23] and screened-exchange (sX) (Ref. 26) methods show that the valence band is formed predominantly by $2p$ oxygen states hybridized with the Fe $3d$ and Bi $6p$ states. The lowest conduction band is formed by the Fe $3d$ states with a density of states (DOS) peak at 3.0 eV followed by the Bi $6p$ states with a DOS distributed from 3 to 6 eV. Most recent calculations give an indirect-band gap E_g=2.8 eV.[26] In contrast to direct-band semiconductors, a strict definition of the band-gap value E_g in transition-metal compounds from experimental data is not straightforward. It is complicated by the absence of a sharp absorption edge and therefore depends on the procedure adopted. The experimental estimate based on optical-absorption measurements in $BiFeO_3$ thin films gives a band gap E_g=2.5 eV.[21] More recent estimates give a direct-band gap E_g=2.7 eV (Refs. 20, 27, and 28) or E_g=2.8 eV.[22]

However, this kind of estimate is strongly dependent on sample morphology and quality.

The low-energy optical response in bismuth ferrite $BiFeO_3$ reveals puzzling features, pointing to a CT instability in that oxide. It is an enhanced structureless spectral weight in a wide range below the main CT bands in $BiFeO_3$ with a remarkable smearing of the fundamental edge. The anomaly may be assigned to CT instabilities accompanied by the self-trapping of *p-d* CT excitons and the nucleation of electron-hole droplets. Indeed, the main optical response of the self-trapped *p-d* CT excitons is determined by the electron-hole recombination process $Fe^{2+}O^{1-} \rightarrow Fe^{3+}O^{2-}$, which energy is surely smaller than the energy of a direct CT process $Fe^{3+}O^{2-} \rightarrow Fe^{2+}O^{1-}$.

Despite the orthorhombic crystal symmetry of the iron borate Fe_3BO_6, its optical response resembles in general features that of trigonal hematite but not that of orthoferrites. One should note a strong anisotropy especially pronounced for the low-energy intense $t_{2u}(\pi) \rightarrow t_{2g}$ band which looks like a solitary peak at 3 eV in the *b* polarization [Fig. 6(c)] and transforms into a plateau for the *a* and *c* polarizations, seemingly composed of two bands peaked at 3.2 and 4.2 eV. Such a strong anisotropy indirectly supports the *p-d* CT nature of the optical response. Indeed, unusually strong, up to ~20%, distortions of FeO_6 octahedra in Fe_3BO_6 (Refs. 56 and 57) imply a large low-symmetry splitting of both the initial $t_{2u}(\pi)$ and final t_{2g} states. The resultant effect may be strong enough to explain a splitting on the order of 1 eV. Iron borate spectra provide again a clear evidence of the 2.5 eV band assigned to dipole-forbidden *p-d* CT transitions $t_{1g}(\pi) \rightarrow t_{2g}$. Indeed, the well-pronounced low-energy spectral features are clearly seen at 2.26 and 2.56 eV in *b* polarization. Most probably the low-symmetry effects are the main source responsible for the crucial difference in the optical response between Fe_3BO_6 and two other iron borates $FeBO_3$ (T_N = 348 K) and $GdFe_3(BO_4)_3$ (T_N = 37 K).[60,61] These two borates are highly transparent in the visible spectral range and the CT bands are less intense and shifted to higher photon energy. Interestingly that at variance with most of ferrites where the Fe-O-Fe bonds form a three-dimensional network, the main motives of the crystal structure in $GdFe_3(BO_3)_4$ are spiral chains of FeO_6 octahedra running along the *c* axis and linked together by their edges. The antiferromagnetic ordering of the Fe subsystem occurs at about 37 K. In such a system, one might observe the *d-d* CT transitions for the polarization $\mathbf{E} \| c$ axis. Indeed, the absorption spectrum of $GdFe_3(BO_3)_4$ reveals an intensive band peaked near 4.8 eV observed for $\mathbf{E} \| c$ axis,[61] which may be attributed to the $e_g - t_{2g}$ CT transition in pairs of Fe^{3+} ions running along the *c* axis.

The optical response of ferrites containing both octahedral FeO_6 and tetrahedral FeO_4 centers is more complicated for a comprehensive analysis. First of all, we should point to a sizable (~0.5 eV) blueshift of the onset energy for the *p-d* CT transitions in tetrahedral FeO_4 centers as compared to the octahedral FeO_6 centers.[76,77] This makes the low-energy optical response in such ferrites to be similar to that of ferrites with only octahedral FeO_6 centers.

Optical spectra of $LiFe_5O_8$ resemble those of hematite up to a quantitative agreement. Low-energy spectral features at 2.4 and 2.56 eV coincide with those observed in the spectral dependencies of its circular dichroism[11] and linear Kerr effect.[64] They were assigned to the *d*−*d* transitions in the Fe^{3+} ions in the octahedral and tetrahedral positions, respectively. However, their assignment to a split dipole-forbidden $t_{1g} - t_{2g}$ CT transition seems to be more reasonable, especially because such 2.5 eV band is typical for other octa/tetraferrites (see Figs. 7 and 8).

The optical response of calcium ferrite $Ca_2Fe_2O_5$ reveals a striking difference from the spectra of all other materials discussed above. The most noticeable feature is a strong suppression of the "octahedral" 3 eV band with a puzzling redshift of the respective spectral weight, which forms an extensive low-energy tail of the 3 eV band and anomalously strong midinfrared band peaked below 1 eV. Both anomalies are believed to indicate a well-developed CT instability of calcium ferrite due to self-trapping of the *p-d* CT excitons in octahedral Fe^{3+} centers similar to that of bismuth ferrite. The strong redshift of their spectral weight for the respective *p-d* CT excitons makes manifestation of tetrahedral FeO_4 centers more pronounced. The significant optical anisotropy observed in $Ca_2Fe_2O_5$ can be attributed to a manifestation of the interlayer octa-tetra *d-d* CT transitions with the $\mathbf{E} \| b$-axis polarization. Indeed, calcium ferrite has a typical pseudoquadratic layered structure with alternating layers of highly symmetrical octahedral and tetrahedral Fe^{3+} centers having similar projections along the *a* and *c* axes (see Figs. 2 and 3 in Ref. 71). The peak energy of 4.1 eV for the respective band agrees with our estimates for *d-d* CT transitions.

In the discussion above, we have focused on the more or less intensive CT bands, leaving out manifestations of the essentially weaker crystal-field transitions, part of which is superposed on the stronger CT bands. First of all, it concerns a generic ${}^6A_{1g} \rightarrow {}^4A_{1g}$ transition which is usually superposed on the dipole-forbidden $t_{1g}(\pi) - t_{2g}$ *p-d* CT transition.

V. CHARGE TRANSFER INSTABILITY AND PROBABLE METAL-INSULATOR TRANSITION IN $BiFeO_3$

The relation between the minimal energies of *p-d* and *d-d* CT transitions is of great importance for any insulating 3*d* oxide. Zaanen *et al.*[78] developed a general framework for oxides, according to which there are two types of insulators: the Mott insulators with the smallest *d-d* CT energy and the charge transfer insulators with the smallest *p-d* CT energy, respectively. Accordingly, they introduce two types of metal-insulator transitions with the closing of the Mott-Hubbard *d-d* CT gap and of the *p-d* CT gap, respectively. All the iron oxides addressed in our paper may be classified as CT insulators where the CT gap is determined by the dipole-forbidden $t_{1g} \rightarrow t_{2g}$ (*p-d*) CT transition. This point merits to be especially emphasized in connection with the usual procedure of optical detection of the CT or insulating gap.

Actually, we should distinguish between the optical and thermal or conductivity gap. Indeed, the minimal energy cost of the optically excited *p-d* CT transition in insulating ferrites is 2.5–3.0 eV. The question arises: what is the minimal energy cost for the thermal excitation of such a local CT and what is the respective electronic state? The answer implies,

first of all, a knowledge of the relaxation energy to be a cumulative (of several eV) effect of *electronic* and *ionic* terms associated with the displacement of electron shells and ionic cores, respectively.[38] Some hints regarding this relaxation effect can be obtained by reviewing the in-gap low-energy optical response. The observation of midinfrared CT bands and the enhanced spectral weight in a wide range below the main CT bands, with a remarkable smearing of the fundamental edge, point to CT instabilities accompanied by the self-trapping of *p-d* CT excitons and the nucleation of electron-hole droplets. All these optical features are typical for ferrites. Moreover, the analysis of the spectral weight redistribution in bismuth ferrite $BiFeO_3$ and, in particular, in calcium ferrite $Ca_2Fe_2O_5$ shows that the in-gap optical features may be related to a self-trapped *p-d* CT exciton in octahedral FeO_6 centers that is responsible for the generic 3 eV CT band.

What is the ground state of the relaxed metastable *p-d* electron-hole center in ferrites? A simple overview of the Tanabe-Sugano diagram for $3d^6$ configuration of Fe^{2+} ion points to two candidate "relaxed-excited CT states" to compete for stability with the ground state,

$$[FeO_6]^{9-}(t_{2g}^3 e_g^2; {}^6A_{1g}) \rightarrow \begin{cases} [FeO_6]^{9-}(t_{2g}^4 e_g^2; {}^5T_{2g}:\underline{t}_{1g}) \\ [FeO_6]^{9-}(t_{2g}^6; {}^1A_{1g}:\underline{t}_{1g}). \end{cases}$$

The high-spin $t_{2g}^4 e_g^2; {}^5T_{2g}:\underline{t}_{1g}(\pi)$ and zero-spin $t_{2g}^6; {}^1A_{1g}:\underline{t}_{1g}(\pi)$ configurations are stabilized at weak and strong crystal fields, respectively. One should note that the bare "ionic" state corresponds to a sufficiently longer equilibrium Fe-O bond length than the "covalent" CT state with an oxygen hole. This indicates a specific role played by the breathing mode in the CT exciton self-trapping effect accompanied by charge fluctuations. On the other hand, it implies that the CT exciton self-trapping can be governed by the lattice contraction/strain. The *p-d* CT configurations with oxygen holes are believed to form a metallic phase, thus providing a natural route to a metal-insulator transition under specific external conditions such as high pressure or high temperature.

Apart from the *p-d* CT states, there are other candidate states to compete for a ground state of the FeO_6 octahedra. First, there is a low-spin $S=1/2$ state $t_{2g}^5; {}^2T_{2g}$ which is stabilized by a strong crystal field, for instance, under high pressure. When pressure is applied, the ligand field strength increases as a result of the M-O distance shortening. At a critical pressure, the ligand field strength $10Dq$ will overcome the Hund *d-d* interaction and the high-spin $S=5/2$ ground state ${}^6A_{1g}$ of Fe^{3+} ion will be replaced by the low-spin $S=1/2$ ground-state ${}^2T_{2g}$.

The high-spin-low-spin (HS-LS) phase transition is not necessarily accompanied by a metal-insulator transition but leads to a system with lower spin and magnetic moment due to a rearrangement of electrons in the outermost electronic orbitals. Their isostructural nature implies that no modification of crystal symmetry should be observed but rather changes associated with modifications of the internal degrees of freedom in the unit cell, as a result of the change in chemical bonding between the anions and cations induced by such radical electronic transformations.

The HS-LS phase transition accompanied by a collapse of the local magnetic moment has been observed at high pressure near 50 GPa in a number of ferrites $FeBO_3$,[79] $BiFeO_3$,[18] $LaFeO_3$,[80] $(La,Pr)FeO_3$,[81] $NdFeO_3$,[82] Fe_2O_3,[83] $GdFe_3(BO_3)_4$,[84] and $Y_3Fe_5O_{12}$.[85] However, only in $BiFeO_3$ this transition is accompanied by a metal-insulator transition. Detailed high-pressure studies of structural, electronic, and magnetic properties of $BiFeO_3$ crystal have been performed in Ref. 18. The reversible metal-insulator transition was observed at room temperature at pressures higher than 55 GPa. The metal-insulator transition was assumed to be induced by the HS-LS crossover in the Fe^{3+} ion subsystem, which drives the effective correlation energy U_{eff} below the threshold for the transition.

It is interesting that the metal-insulator transition in $BiFeO_3$ can be driven by temperature. Extensive high-temperature experimental studies of multiferroic bismuth ferrite $BiFeO_3$ were performed in Ref. 19. The authors report a rhombohedral-orthorhombic-cubic phase-transition sequence between 820 °C and 930 °C. The transition to the cubic phase causes an abrupt collapse of the band gap toward zero and a metal-insulator transition at the orthorhombic-cubic transition around 930 °C. The metallic state was assumed to be triggered by a big lattice contraction. They find that the same cubic phase of $BiFeO_3$, as is measured at atmospheric pressure at 931 °C, is also reached at room temperature and at a hydrostatic pressure of about 47 GPa. The true nature of the metal-insulator transition in $BiFeO_3$ remains unknown; however, the *p-d* CT scenario seems to be one of the most probable, taking into account the particularly strong electron-lattice polarization effects in this ferroelectric compound. On the other hand, the low-spin $Fe^{3+}(t_{2g}^5; {}^2T_{2g})$ state appears to be unstable with regard to a disproportionation reaction

$$[FeO_6]^{9-}(t_{2g}^5; {}^2T_{2g}) + [FeO_6]^{9-}(t_{2g}^5; {}^2T_{2g}) \rightarrow [FeO_6]^{8-}(t_{2g}^3 e_g^1; {}^5E_g) + [FeO_6]^{10-}(t_{2g}^4 e_g^2; {}^2T_{2g})$$

that points to another route to form a metalliclike system of hole and electron centers.

The CT instability revealed by optical measurements can be closely related to a multiferroicity due to a strong electric polarizability of the self-trapped CT excitons and EH droplets and their magnetic-order-dependent volume fraction.

VI. CONCLUSIONS

We have reported the results of a comprehensive theoretical and experimental study of different CT transitions in the multiferroic $BiFeO_3$ and related complex iron oxides. The optical response was studied in a wide spectral range from 0.6 up to 5.8 eV by means of spectroscopic ellipsometry. The iron oxides investigated have different crystal symmetry with more or less distorted FeO_6 octahedral and FeO_4 tetrahedral centers. One of the two groups of materials includes $BiFeO_3$, $ErFeO_3$, $Y_{.95}Bi_{.05}FeO_3$, α-Fe_2O_3, $Fe_{2-x}Ga_xO_3$, and Fe_3BO_6 in which iron Fe^{3+} ions occupy only octahedral centrosymmetric or noncentrosymmetric positions with different magni-

tude of distortions from 1–20 %. The second group includes $LiFe_5O_8$, $BaFe_{12}O_{19}$, $Sm_3Fe_5O_{12}$, and $Ca_2Fe_2O_5$ in which Fe^{3+} ions occupy both octahedral and tetrahedral positions with a rising tetra/orthoratio. All compounds studied possess high Néel or Curie temperatures. We show that in spectral range up to ~3.7 eV, the optical response is dominated by the *p-d* CT transitions, while at $E > 3.7$ eV both *p-d* and *d-d* CT transitions are revealed.

At variance with several previous investigations, we present a unified assignment of different dipole-allowed and dipole-forbidden CT transitions. All the ferrites investigated are qualified to be CT insulators with the band gap determined by a dipole-forbidden *p-d* CT transition $t_{1g} \rightarrow t_{2g}$ near 2.5 eV, the spectral weight of which is strongly enhanced for the ferrites $BiFeO_3$ and α-Fe_2O_3 with noncentrosymmetric distortion of FeO_6 octahedra. In other words, the weak 2.5 eV band superimposed on the tail of the strong 3.0 eV band has a "nondefect" intrinsic nature and, along with the latter, can be addressed to be a visiting card of the octahedral FeO_6 centers. It means we should revisit our view on the band-gap structure in all the ferrites.

Intense bands near 3.0 and 4 eV are assigned to dipole-allowed $t_{2u}(\pi) \rightarrow t_{2g}$ and $t_{1u}(\pi) \rightarrow t_{2g}$ (*p-d*) CT transitions in octahedral FeO_6 centers, respectively. The assignment of the low-energy two-center $e_g \rightarrow t_{2g}$ $^6A_{1g}{}^6A_{1g} \rightarrow {}^5E_g{}^5T_{2g}$ (*d-d*) CT transition to an unconventional Jahn-Teller-like final state, with an orbital degeneracy on both sites, is particularly manifested in the orthoferrite $ErFeO_3$ as an intense broad band peaked near 4.5 eV with a narrow low-energy satellite peaked at 3.9 eV. A noticeable enhancement of the optical response in $BiFeO_3$ at ~4 eV as compared to other related iron oxides is attributed to the CT transitions within the Bi-O bonds.

We report an observation of the enhanced structureless spectral weight in a wide range below the main CT bands in $BiFeO_3$ and calcium ferrite $Ca_2Fe_2O_5$, with a remarkable smearing of the fundamental edge. Moreover, calcium ferrite $Ca_2Fe_2O_5$ reveals an unexpected midinfrared CT band. All these anomalies are assigned to CT instabilities accompanied by the self-trapping of *p-d* CT excitons and nucleation of the electron-hole droplets. The optical detection of CT instability agrees with the observation of a metal-insulator transition in bismuth ferrite. We suppose the CT instability be closely related to multiferroicity due to a strong electric polarizability of the self-trapped CT excitons and EH droplets and their magnetic-order-dependent volume fraction. We believe that the results of our paper give deeper insight into the electronic structure of the iron oxide multiferroics and related ferrite compounds and provide a solid basis for the further experimental and theoretical work on the topic.

ACKNOWLEDGMENTS

We thank A. F. van Etteger and A. J. Toonen for technical support and V. V. Pavlov for the help in the data analysis. We thank A. M. Balbashov for orthoferrite single crystals and L. N. Bezmaternykh for iron borate single crystals. This work is supported by the Russian Foundation for Basic Research, the Dutch Nanotechnology Network NanoNed, de Nederlandse Organisatie voor Wetenschappelijk Onderzoek NWO, INTAS, and FP7 under the grant N214810 (FANTOMAS).

[1] G. A. Smolenskii and I. E. Chupis, Usp. Fiz. Nauk **137**, 415 (1982) [Sov. Phys. Usp. **25**, 475 (1982)].
[2] M. Fiebig, J. Phys. D **38**, R123 (2005).
[3] W. Eerenstein, N. D. Mathur, and J. F. Scott, Nature (London) **442**, 759 (2006).
[4] A. B. Harris, Phys. Rev. B **76**, 054447 (2007).
[5] M. Fiebig, D. Fröhlich, K. Kohn, S. Leute, T. Lottermoser, V. V. Pavlov, and R. V. Pisarev, Phys. Rev. Lett. **84**, 5620 (2000).
[6] T. Kimura, T. Goto, H. Shintani, K. Ishizaka, T. Arima, and Y. Tokura, Nature (London) **426**, 55 (2003).
[7] N. Hur, S. Park, P. A. Sharma, J. S. Ahn, S. Guha, and S.-W. Cheong, Nature (London) **429**, 392 (2004).
[8] K. Saito and K. Kohn, J. Phys.: Condens. Matter **7**, 2855 (1995).
[9] H. Kimura, S. Kobayashi, S. Wakimoto, Y. Noda, and K. Kohn, Ferroelectrics **354**, 77 (2007).
[10] G. T. Rado, Phys. Rev. Lett. **13**, 335 (1964).
[11] V. N. Gridnev, B. B. Krichevtsov, V. V. Pavlov, and R. V. Pisarev, JETP Lett. **65**, 68 (1997).
[12] B. B. Krichevtsov, V. V. Pavlov, and R. V. Pisarev, JETP Lett. **49**, 535 (1989).
[13] T. Arima, D. Higashiyama, Y. Kaneko, J. P. He, T. Goto, S. Miyasaka, T. Kimura, K. Oikawa, T. Kamiyama, R. Kumai, and Y. Tokura, Phys. Rev. B **70**, 064426 (2004).
[14] K. Eguchi, Y. Tanabe, T. Ogawa, M. Tanaka, Y. Kawabe, and E. Hanamura, J. Opt. Soc. Am. B **22**, 128 (2005).
[15] A. M. Kalashnikova, R. V. Pisarev, L. N. Bezmaternykh, V. L. Temerov, A. Kirilyuk, and Th. Rasing, JETP Lett. **81**, 452 (2005).
[16] T. Kimura, G. Lawes, and A. P. Ramirez, Phys. Rev. Lett. **94**, 137201 (2005).
[17] S. Ishiwata, Y. Taguchi, H. Murakava, Y. Onose, and Y. Tokura, Science **319**, 1643 (2008).
[18] A. G. Gavriliuk, V. V. Struzhkin, I. S. Lyubutin, S. G. Ovchinnikov, M. Y. Hu, and P. Chow, Phys. Rev. B **77**, 155112 (2008).
[19] R. Palai, R. S. Katiyar, H. Schmid, P. Tissot, S. J. Clark, J. Robertson, S. A. T. Redfern, G. Catalan, and J. F. Scott, Phys. Rev. B **77**, 014110 (2008).
[20] S. R. Basu, L. W. Martin, Y. H. Chu, M. Gajek, R. Ramesh, R. C. Rai, X. Xu, and J. L. Musfeldt, Appl. Phys. Lett. **92**, 091905 (2008).
[21] T. Kanai, S. Ohkoshi, and K. Hashimoto, J. Phys. Chem. Solids **64**, 391 (2003).
[22] A. Kumar, R. C. Rai, N. J. Podraza, S. Denev, M. Ramirez, Y. H. Chu, L. W. Martin, J. Ihlefeld, T. Heeg, J. Schubert, D. G. Schlom, J. Orenstein, R. Ramesh, R. W. Collins, J. L. Musfeldt, and V. Gopalan, Appl. Phys. Lett. **92**, 121915 (2008).
[23] J. B. Neaton, C. Ederer, U. V. Waghmare, N. A. Spaldin, and K. M. Rabe, Phys. Rev. B **71**, 014113 (2005).

[24] P. Baettig, C. Ederer, and N. A. Spaldin, Phys. Rev. B **72**, 214105 (2005).
[25] C. Ederer and N. A. Spaldin, Phys. Rev. B **71**, 060401(R) (2005).
[26] S. J. Clark and J. Robertson, Appl. Phys. Lett. **90**, 132903 (2007).
[27] A. J. Hauser, J. Zhang, L. Mier, R. A. Ricciardo, P. M. Woodward, T. L. Gustafson, L. J. Brillson, and F. Y. Yang, Appl. Phys. Lett. **92**, 222901 (2008).
[28] J. F. Ihlefeld, N. J. Podraza, Z. K. Liu, R. C. Rai, X. Xu, T. Heeg, Y. B. Chen, J. Li, R. W. Collins, J. L. Musfeldt, X. Q. Pan, J. Schubert, R. Ramesh, and D. G. Schlom, Appl. Phys. Lett. **92**, 142908 (2008).
[29] S. Picozzi, K. Yamauchi, B. Sanyal, I. A. Sergienko, and E. Dagotto, Phys. Rev. Lett. **99**, 227201 (2007).
[30] A. S. Moskvin and S.-L. Drechsler, Phys. Rev. B **78**, 024102 (2008).
[31] Y. Tanabe, T. Moriya, and S. Sugano, Phys. Rev. Lett. **15**, 1023 (1965).
[32] A. S. Moskvin and R. V. Pisarev, Phys. Rev. B **77**, 060102(R) (2008).
[33] F. J. Kahn, P. S. Pershan, and J. P. Remeika, Phys. Rev. **186**, 891 (1969).
[34] A. I. Liechtenshtein, A. S. Moskvin, and V. A. Gubanov, Sov. Phys. Solid State **24**, 2049 (1982).
[35] A. S. Moskvin, Phys. Rev. B **65**, 205113 (2002).
[36] N. N. Kovaleva, A. V. Boris, C. Bernhard, A. Kulakov, A. Pimenov, A. M. Balbashov, G. Khaliullin, and B. Keimer, Phys. Rev. Lett. **93**, 147204 (2004).
[37] D. A. Varshalovich, A. N. Moskalev, and V. K. Khersonskii, *Quantum Theory of Angular Momentum* (World Scientific, Singapore, 1988).
[38] A. L. Shluger and A. M. Stoneham, J. Phys.: Condens. Matter **5**, 3049 (1993).
[39] N. N. Kovaleva, J. L. Gavartin, A. L. Shluger, A. V. Boris, and A. M. Stoneham, JETP **94**, 178 (2002).
[40] A. S. Moskvin, J. Phys.: Conf. Ser. **21**, 106 (2005).
[41] A. S. Moskvin, Low Temp. Phys. **33**, 234 (2007).
[42] A. M. Balbashov and S. K. Egorov, J. Cryst. Growth **52**, 498 (1981).
[43] A. M. Kalashnikova and R. V. Pisarev, JETP Lett. **78**, 143 (2003).
[44] P. A. Usachev, R. V. Pisarev, A. M. Balbashov, A. V. Kimel, A. Kirilyuk, and T. Rasing, Phys. Solid State **47**, 2292 (2005).
[45] R. M. A. Azzam and N. M. Bashara, *Ellipsompetry and Polarized Light* (North-Holland, Amsterdam, 1977).
[46] D. E. Aspnes, J. Opt. Soc. Am. **70**, 1275 (1980).
[47] G. E. Jellison, Jr., and J. S. Baba, J. Opt. Soc. Am. A Opt. Image Sci. Vis **23**, 468 (2006).
[48] M. Adachi, Y. Akishige, T. Asahi, *et al.*, in *Landolt-Börnstein, Numerical Data and Functional Relationships in Science and Technology*, New Series-Group III Condensed Matter Vol. 36A1 (Springer-Verlag, Berlin, 2002).
[49] F. Kubel and H. Schmid, Acta Crystallogr., Sect. B: Struct. Sci. **46**, 698 (1990).
[50] A. Palewicz, R. Przenioslo, I. Sosnovska, and A. W. Hewat, Acta Crystallogr., Sect. B: Struct. Sci **63**, 537 (2007).
[51] J. F. Scott, M. K. Singh, and R. S. Katiyar, J. Phys.: Condens. Matter **20**, 322203 (2008).
[52] Y. Endoh, K. Kakurai, A. K. Katori, *et al.*, in *Landolt-Börnstein, Numerical Data and Functional Relationships in Science and Technology*, New Series: Group III Condensed Matter Vol. 27F3 (Springer-Verlag, Berlin, 1994).
[53] J. P. Rivera and H. Schmid, Ferroelectrics **204**, 23 (1997).
[54] R. L. Blake, R. E. Hessevick, T. Zoltai, and L. W. Finger, Am. Mineral. **51**, 123 (1966).
[55] D. Bonnenberg, K. A. Hempel, R. A. Lefever *et al.*, in *Landolt-Börnstein Numerical Data and Functional Relationships in Science and Technology*, New Series: Group III Condensed Matter Vol. 12B (Springer-Verlag, Berlin, 1980).
[56] J. G. White, A. Miller, and R. E. Nielsen, Acta Crystallogr. **19**, 1060 (1965).
[57] R. Diehl and G. Brandt, Acta Crystallogr. B **31**, 1662 (1975).
[58] E. Burzo in *Landolt-Börnstein, Numerical Data and Functional Relationships in Science and Technology*, New Series–Group III: Condensed Matter, Vol. 27H (Springer-Verlag, Berlin, 1993).
[59] B. Andlauer, R. Diehl, and M. S. Skolnik, J. Appl. Phys. **49**, 2200 (1978).
[60] P. A. Markovin, A. M. Kalashnikova, R. V. Pisarev, and T. Rasing, JETP Lett. **86**, 712 (2007).
[61] A. M. Kalashnikova, V. V. Pavlov, R. V. Pisarev, L. N. Bezmaternyukh, M. Bayer, and T. Rasing, JETP Lett. **80**, 293 (2004).
[62] C. Wende and H. Langbein, Cryst. Res. Technol. **41**, 18 (2006).
[63] M. I. Bichurin, V. M. Petrov, Yu. V. Kiliba, and G. Srinivasan, Phys. Rev. B **66**, 134404 (2002).
[64] S. Višnovsky, R. Krishnan, V. Prosser, N. P. Thuy, and I. Stroda, Appl. Phys. (Berlin) **18**, 243 (1979).
[65] R. R. Arons, D. Bonnenberg, P. Grünberg *et al.*, in *Landolt-Börnstein, Numerical Data and Functional Relationships in Science and Technology*, New Series-Group III: Condensed Matter Vol. 12C (Springer-Verlag, Berlin, 1982).
[66] K. Enke, J. Fleischhauer, W. Gunsser *et al.*, in *Landolt-Börnstein, Numerical Data and Functional Relationships in Science and Technology*, New Series-Group III: Condensed Matter, Vol. 12A (Springer-Verlag, Berlin, 1978).
[67] G. Winkler, *Magnetic Garnets* (Vieweg and Son, Braunschweig, Germany, 1981).
[68] G. B. Scott, D. E. Lacklison, and J. L. Page, Phys. Rev. B **10**, 971 (1974).
[69] S. Wittekoek, T. J. A. Popma, J. M. Robertson, and P. F. Bongers, Phys. Rev. B **12**, 2777 (1975).
[70] E. Burzo in *Landolt-Börnstein, Numerical Data and Functional Relationships in Science and Technology*, New Series-Group III: Condensed Matter , Vol. 27F1a (Springer-Verlag, Berlin, 1996).
[71] E. F. Bertaut, P. Blum, and A. Sagniéres, Acta Crystallogr. **12**, 149 (1959).
[72] P. Marchukov, R. Geick, C. Brotzeller, W. Treutmann, E. G. Rudashevsky, and A. M. Balbashov, Phys. Rev. B **48**, 13538 (1993).
[73] H. D. Zhou and J. B. Goodenough, Solid State Sci. **7**, 656 (2005).
[74] C. B. Azzoni, M. C. Mozzatti, V. Massarotti, D. Capsoni, and M. Bini, Solid State Sci. **9**, 515 (2007).
[75] W. Jung, J. Appl. Phys. **36**, 1249 (1965).
[76] A. S. Moskvin, A. V. Zenkov, E. I. Yuryeva, and V. A. Gubanov, Physica B **168**, 187 (1991).
[77] A. S. Moskvin, A. V. Zenkov, E. A. Ganshina, G. S. Krinchik, and M. M. Nishanova, J. Phys. Chem. Solids **54**, 101 (1993).
[78] J. Zaanen, G. A. Sawatzky, and J. W. Allen, Phys. Rev. Lett. **55**,

418 (1985).
[79] I. A. Trojan, M. I. Eremets, A. G. Gavriliuk, I. S. Lyubutin, and V. A. Sarkisyan, JETP Lett. **78**, 16 (2003).
[80] G. R. Hearne, M. P. Pasternak, R. D. Taylor, and P. Lacorre, Phys. Rev. B **51**, 11495 (1995).
[81] W. M. Xu, O. Naaman, G. Kh. Rozenberg, M. P. Pasternak, and R. D. Taylor, Phys. Rev. B **64**, 094411 (2001).
[82] A. G. Gavriliuk, I. A. Troyan, R. Boehler, M. I. Eremets, I. S. Lyubutin, and N. R. Serebryanaya, JETP Lett. **77**, 619 (2003).
[83] J. Badro, G. Fiquet, V. V. Struzhkin, M. Somayazulu, H. K. Mao, G. Shen, and T. LeBihan, Phys. Rev. Lett. **89**, 205504 (2002).
[84] A. G. Gavriliuk, S. A. Kharlamova, I. S. Lyubutin, I. A. Troyan, S. G. Ovchinnikov, A. M. Potseluiko, M. I. Eremets, and R. Boehler, JETP Lett. **80**, 426 (2004).
[85] I. S. Lyubutin, A. G. Gavriliuk, I. A. Trojan, and P. A. Sadykov, JETP Lett. **82**, 702 (2005).